

FragPT2: multifragment wave function embedding with perturbative interactions

Koridon, E.F.; Sen, S.; Visscher, L.; Polla, S.

Citation

Koridon, E. F., Sen, S., Visscher, L., & Polla, S. (2025). FragPT2: multifragment wave function embedding with perturbative interactions. *Journal Of Chemical Theory And Computation*, 21(2), 655-669. doi:10.1021/acs.jctc.4c01221

Version: Publisher's Version

License: <u>Creative Commons CC BY 4.0 license</u>
Downloaded from: <u>https://hdl.handle.net/1887/4281849</u>

Note: To cite this publication please use the final published version (if applicable).



pubs.acs.org/ICTC Article

FragPT2: Multifragment Wave Function Embedding with **Perturbative Interactions**

Emiel Koridon,* Souloke Sen, Lucas Visscher, and Stefano Polla



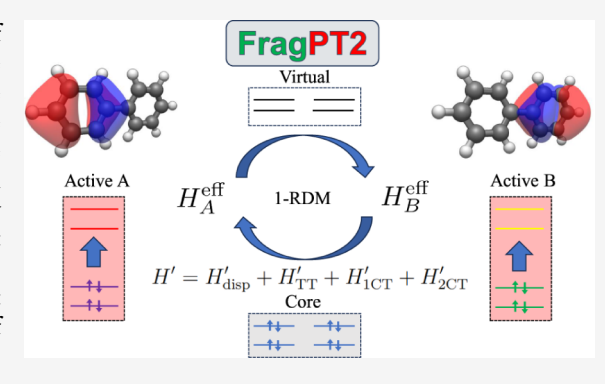
Cite This: J. Chem. Theory Comput. 2025, 21, 655-669



ACCESS I

Metrics & More

ABSTRACT: Embedding techniques allow the efficient description of correlations within localized fragments of large molecular systems while accounting for their environment at a lower level of theory. We introduce FragPT2: a novel embedding framework that addresses multiple interacting active fragments. Fragments are assigned separate active spaces, constructed by localizing canonical molecular orbitals. Each fragment is then solved with a multireference method, self-consistently embedded in the mean field from other fragments. Finally, interfragment correlations are reintroduced through multireference perturbation theory. Our framework provides an exhaustive classification of interfragment interaction terms, offering a tool to analyze the relative importance of various processes such as dispersion, charge transfer, and spin exchange. We benchmark FragPT2 on challenging test systems, including N₂



Article Recommendations

dimers, multiple aromatic dimers, and butadiene. We demonstrate that our method can be successful even for fragments defined by cutting through a covalent bond.

1. INTRODUCTION

Downloaded via LEIDEN UNIV on November 4, 2025 at 06:46:59 (UTC). See https://pubs.acs.org/sharingguidelines for options on how to legitimately share published articles.

Multiconfigurational (MC) wave function-based methods have long been the workhorse of ab initio quantum chemistry, particularly for systems with low-lying or degenerate electronic states.^{1,2} Practical MC approaches, such as the complete active space self-consistent field (CASSCF),³ require defining an active space comprising a subset of the most chemically relevant orbitals. Within this space, electron correlations are calculated exactly by a configuration interaction (CI) wave function, a superposition of all electronic configurations formed from a given set of active electrons and orbitals. The number of these configurations scales exponentially with the size of the active space, limiting the application of these methods to small systems. There have been substantial efforts to expand the size of the active space: some try to restrict the number of excitations by partitioning the active space, 4-9 others involve adaptive procedure to select the configurations with the largest weights. 10,11 Radically different approaches to constructing a compressed CI wave function include tensornetwork algorithms such as the density matrix renormalization group (DMRG), 12 quantum Monte Carlo (QMC) methods, 13 or various kinds of quantum algorithms. 14

A more pragmatic approach for extending multiconfigurational computations to larger systems relies on the concepts of fragmentation and embedding. 15-18 Fragmentation exploits the inherent locality of the problem, describing a system as a composition of simpler subsystems. Each subsystem is then treated with a higher level of theory. The subsystems are then

recombined by embedding them in each other's environment at a lower level of theory. The subsystem orbitals can be constructed in various ways, with the most prominent method being Density Matrix Embedding Theory (DMET). 19-22 DMET constructs fragment and bath orbitals based on the Schmidt decomposition of a trial low-level (e.g., Hartree-Fock) single-determinant wave function of the full system. A high-level calculation (e.g., FCI, Coupled-Cluster, 23,24 CASSCF,²⁵ DMRG,^{24,26,27} or auxiliary-field QMC²⁸ is then performed on the fragment orbitals. Subsequently, the lowlevel wave function is fine-tuned self-consistently via the introduction of a local correlation potential. Fragmentation and embedding have also been studied in the context of DFT.^{29,30} MC wave function-based methods that explicitly construct localized active spaces for each fragment include the Active Space Decomposition method,³¹ cluster Mean Field (cMF)³² and Localized Active Space Self-Consistent Field (LASSCF).33,34

While fragmentation methods have shown success in reducing the complexity in treating localized static correlations,

Received: September 17, 2024 Revised: December 21, 2024 Accepted: December 23, 2024 Published: January 10, 2025





they typically do not capture interfragment correlations. Especially weak, dynamical, correlations between the different fragments and between fragments and their environment can be crucial for obtaining an accurate description of the full system. In CAS methods, the fragment-environment correlations can be retrieved using Multi-Reference Perturbation Theory (MRPT)³⁶ methods like Complete Active Space Second-Order Perturbation Theory (CASPT2)³⁷ and N-Electron Valence Second-Order Perturbation Theory (NEVPT2). Some methods have been developed to also recover interfragment correlations in embedding schemes either variationally, perturbatively, perturbatively, or via a coupled-cluster approach. Although treating strong correlations between fragments remains challenging, there has been some work in this direction. Although treating strong correlations are ecent work proposed to treat interfragment entanglement with a Unitary Coupled Cluster ansatz using the LASSCF framework.

In this work, we introduce and benchmark a novel active space embedding framework, which we call FragPT2. Based on a user-defined choice of two molecular fragments (defined as a partition of the atoms in the molecule), we employ a top-down localization scheme that generates an orthonormal set of localized molecular orbitals, ordered by quasi-energies and assigned to a specific fragment. Using these localized orbitals, we define separate and orthogonal fragment active spaces. Our orbital fragmentation scheme is straightforward, it does not require iterative optimization, and it allows to define fragment orbitals even when the fragments are covalently bonded; on the downside, a good choice of fragments based on chemical intuition is crucial for the success of our method. Within each fragment's active space, we self-consistently find the MC ground state influenced by the mean field of the other fragment (defined as a function of the fragment 1-particle reduced density matrix).

The factorized state obtained with our method has a similar structure to the wave function used in LASSCF and cMF, as these methods also construct product state wave functions of MC states defined on fragmented active spaces. The cMF method is designed for the 1D and 2D Fermi-Hubbard model. It is based on expressing the ground state wave function as a tensor product of many-body states defined on local fragments. The fragment orbitals are then optimized self-consistently to minimize the total energy of the considered product state. Interfragment correlations are then recovered in second-order perturbation theory, using excited fragment eigenstates as perturbing functions. On the other hand, LASSCF exploits a modified DMET algorithm to construct fragments. Starting from a product state, a Schmidt decomposition is used to define fragment and bath orbitals for each fragment. Similarly to cMF, the product state and fragment definition are then optimized self-consistently. The resulting method can be made fully variational with respect to both CI and orbital coefficients.³⁴ In contrast, in our approach, active fragment orbitals are defined in top-down fashion, starting from a set of reference canonical molecular orbitals. Our method is variational with respect to the considered (fragment CI) parameters, and does not require any orbital optimization. As a trade-off for the simplicity of the method, we expect our product wave function to have a higher energy than the orbitaloptimized LASSCF for the same fragment active space sizes. We instead aim to recover the remaining interfragment correlations perturbatively.

To this end, our product state will be used as a starting point for MRPT to recover interfragment correlations. The interactions between fragments can be naturally classified on the basis of charge and spin symmetries imposed on the single fragments, offering analytic insight into the nature of these correlations. Differently from cMF, the perturbing functions are chosen on the basis of electronic excitation operators present in the original electronic Hamiltonian, and organized according to a partially contracted basis akin to MRPT methods like PC-NEVPT2. 38,39 We apply our method to challenging covalently and noncovalently bonded fragments with moderate to strong correlation, providing qualitative estimates of the contributions from various perturbations to the total correlation energy within the active space.

The rest of this paper is organized as follows: in Section 2 we detail our FragPT2 algorithm for multireference fragment embedding. In Section 3, we perform numerical tests of the method on a range of challenging chemical systems, ranging from the noncovalently bonded but strongly correlated N_2 dimer to covalently bonded aromatic dimers and the butadiene molecule. In Section 4 we present an outlook on future research directions, proposing possible improvements for the method and an application in the field of FragPT2 in the field of variational quantum algorithms. Finally, in Section 5 we give concluding remarks.

2. FRAGPT2 METHOD

In this section, we introduce a novel method for fragmented multireference calculations with perturbative corrections: FragPT2. This method works by dividing the active space of a molecule into localized subspaces that can be treated separately using a MC solver, as illustrated in Figure 1. The cost of MC methods scales quickly with the size of the treated active space (e.g., exponentially in the case of FCI); splitting the system into smaller active spaces allows the treatment of larger systems for an affordable computational cost. In this work, we focus on the special case of two active fragments called A and B; however, our method can be promptly generalized to the multiple fragment case as discussed in Section 4.3. Our method requires the user to define the molecular fragments as an input. The choice of fragmentation should be based on chemical intuition, aiming at minimizing interfragment correlations; a good choice is crucial to the success of the method. Our method allows to recover some interfragment correlations, allowing fragmentations that break a covalent bond (like the one shown in Figure 1 for biphenyl), i.e., where two atoms on either side of a covalent bond are assigned to different fragments. The number of bonds broken in fragmentation should, however, be kept to a minimum.

First, in Section 2.1 we introduce the construction of the localized orbitals and the definition of the fragment active spaces. In Section 2.2 we define fragment Hamiltonians by embedding each fragment in the mean field of the other. Applying separate MC solvers to each fragment Hamiltonian, we show how to obtain a fragment product state $|\Psi_0\rangle$ which will be the reference state for subsequent perturbative expansions. Finally, in Section 2.3 we decompose the full Hamiltonian into a sum of the solved fragment Hamiltonians and a number of interfragment interaction terms. We classify these terms on the basis of fragment symmetries and describe a method to treat them in second-order perturbation theory.

2.1. Construction of Recanonicalized Intrinsic Localized Molecular Orbitals. In order to define the fragment

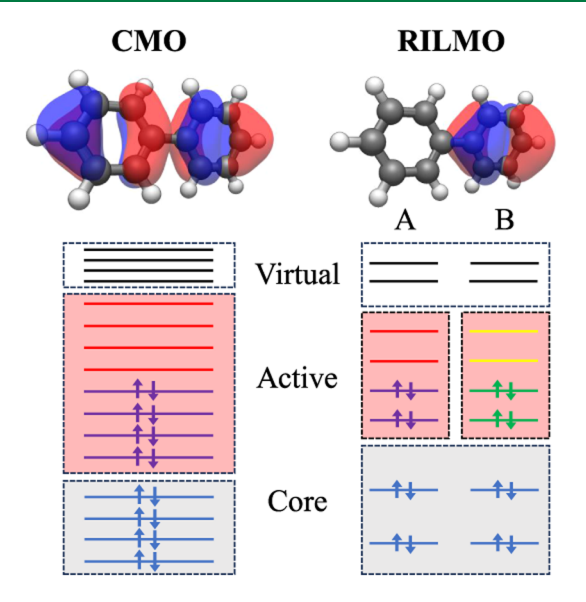


Figure 1. Example of fragmentation and definition of the fragment active spaces. (Left) Active space selection for the entire biphenyl molecule. The CAS treatment separates the canonical molecular orbitals (CMOs) based on their energy ordering, obtaining a set of doubly occupied core orbitals, a set of empty virtual orbitals, and a set of active orbitals around Fermi energy used to describe correlations. We illustrate the highest occupied molecular orbital. (Right) Fragment active space selection for the left and right fragments of the biphenyl molecule. After the localization procedure, we obtain recanonicalized intrinsic localized molecular orbitals (RILMOs), where the orbitals are assigned to either fragment A or B. We can still select core, active, and virtual orbitals for each fragment based on an approximate energy ordering, obtained through the recanonicalization procedure. Here, we depict the highest occupied RILMO for the right fragment. Using our method, we can half the size of the required active space since the multireference solver is applied to just one fragment at a time. The correlations between the localized active spaces can be retrieved afterward with perturbation theory.

subspaces, we follow the top-down procedure introduced in refs. 48 and 49, based on localizing precomputed molecular orbitals. First, we calculate a set of canonical molecular orbitals (CMOs) for the whole system (other choices for molecular orbitals are discussed in Section 5). Distinct Hartree-Fock calculations are also run on each fragment, capped if necessary to saturate bonds severed in the fragmentation. We then choose a valence space, removing a set of hard-core and hardvirtual orbitals far from Fermi energy in both the supermolecular and the fragment calculations. The remaining valence fragment orbitals define the target localized active spaces and are called reference fragment orbitals (RFOs). These RFOs are nonorthogonal and only serve to depolarize the valence CMOs, providing an orthonormal set of intrinsic fragment orbitals (IFOs) of the same dimension as the RFO basis. These IFOs are expressed in the CMO basis and could already be assigned to a particular fragment. They do however mix occupied and virtual spaces and we therefore merely use them to define the localization function in Pipek-Mezey localization 50 of the CMOs. After recanonicalization (blockdiagonalizing the Fock matrix within each fragment), we obtain a set of Recanonicalized Intrinsic Localized Molecular Orbitals (RILMOs), partitioned in fragment subspaces, that together span exactly the occupied space of the original CMOs⁴⁸ plus the chemically relevant valence virtual space. The active spaces for each fragment are illustrated in Figure 1.

In this work we also consider covalently bonded fragments, where there is an ambiguity in assigning one occupied orbital representing the interfragment bond to either fragment. The same ambiguity holds for one unoccupied antibonding orbital, which can also be assigned to either fragment. To eliminate this arbitrariness, we introduce a bias so that any such (anti)bond is always assigned to the first fragment. This enables us to define a natural fragmentation for covalently bonded dimer molecules. As noted already above, in order to generate the required IFO basis for this calculation, we need to deal with "dangling" bonds that are severed in the fragmentation process. For each fragment we simply saturate these by adding a hydrogen atom to the fragment. The thus produced fragment orbitals are well suited as RFOs, but do yield one additional orbital in the span of the RFOs and IFOs. Accepting this feature, the ROSE code reported in ref. 48 could be used without modification. In a forthcoming paper, we plan to discuss the localization of higher lying virtuals for which the RILMO generation does need to be modified (see also ref. 49 for noncovalently bonded subsystems) by removing the capping basis from the RFO space. For the covalently bonded dimer systems tested in this work, the unmodified RILMO generation could be used with only a bias in the selection procedure to assign both the bond and the antibond to the same fragment.

2.2. Fragment Embedding. The total Hamiltonian in the combined active space spanned by both fragments is given by

$$H = \sum_{pq \in A \cup B} h_{pq} E_{pq} + \frac{1}{2} \sum_{pqrs \in A \cup B} g_{pqrs} e_{pqrs}$$

$$\tag{1}$$

where we use the spin-adapted excitation operators

$$\begin{split} E_{pq} &= \sum_{\sigma} a^{\dagger}_{p\sigma} a_{q\sigma} \\ e_{pqrs} &= \sum_{\sigma\tau} a^{\dagger}_{p\sigma} a^{\dagger}_{r\tau} a_{s\tau} a_{q\sigma} = E_{pq} E_{rs} - \delta_{qr} E_{ps}. \end{split} \tag{2}$$

This Hamiltonian includes all interactions of all active orbitals. Our embedding scheme aims at decomposing this Hamiltonian as $H=H^0+H'$, where H^0 includes intrafragment terms and a mean-field interfragment term, and can be solved exactly with separate in-fragment MC solvers. The residual interfragment interactions H' are treated separately with perturbation theory, as described in Section 2.3.

To facilitate the use of separate MC solvers for each fragment, we constrain the wave function of the total system to be a product state over the two fragments,

$$|\Psi^{0}\rangle = |\Psi_{A}\rangle|\Psi_{B}\rangle \tag{3}$$

where $|\Psi_X\rangle$ is a many-body wave function in the active space of fragment X, similar in spirit to cMF and LASSCF. We further restrict each fragment wave function $|\Psi_X\rangle$ to have fixed, integer charge and spin. Note that the conservation of spin and charge on each fragment is not a symmetry of the subsystem; however, this assumption is crucial to construct separate efficient MC solvers. Interfragment charge transfer and spin exchange processes are later treated in perturbation theory.

Under these constraints, we can simplify the expression of H by removing all the terms that do not respect charge and spin conservation on each fragment separately (as their expectation value of $|\Psi^0\rangle$ would anyway be zero). The remaining

Table 1. Summary of the Perturbations and the Cost of PT2^a

	Perturbation	Perturbing functions $\{ \Psi_{\mu\nu}\rangle\}$	Fragment matrix element
1.	$H'_{\text{disp}} = \sum_{pq \in A} \sum_{rs \in B} g'_{pqrs} (E_{pq} - \gamma^A_{pq}) (E_{rs} - \gamma^B_{rs})$	$E_{tu}E_{vw} \Psi^{0}\rangle$ $[tu \in A, vw \in B]$	$\langle \Psi_{\!X} E_{lk} H_X^{\mathrm{eff}} E_{tu} \Psi_{\!X} \rangle$
2.	$H'_{1\text{CT}} = \sum_{p \in A} \sum_{q \in B} \left[h_{pq} - \sum_{r \in A} g_{prrq} \right] E_{pq}$ $+ \sum_{p \in B} \sum_{q \in A} \left[h_{pq} - \sum_{r \in B} g_{prrq} \right] E_{pq}$ $+ \sum_{pqr \in A} \sum_{s \in B} g_{pqrs} E_{pq} [E_{rs} + E_{sr}]$ $+ \sum_{pqr \in B} \sum_{s \in A} g_{pqrs} E_{pq} [E_{rs} + E_{sr}]$	$E_{tu}E_{\nu\nu} \Psi^{0}\rangle$ $\begin{bmatrix} tuv \in A, w \in B \\ tuw \in A, v \in B \\ tuv \in B, w \in A \\ tuw \in B, v \in A \end{bmatrix}$	$\begin{split} \langle \Psi_{\!X} a_m & E_{lk} H_X^{\text{eff}} E_{tu} a_v^\dagger \Psi_{\!X} \rangle \\ \langle \Psi_{\!X} a_m^\dagger E_{lk} H_X^{\text{eff}} E_{tu} a_v \Psi_{\!X} \rangle \end{split}$
3.	$H'_{\text{2CT}} = \frac{1}{2} \sum_{pr \in A} \sum_{qs \in B} g_{pqrs} E_{pq} E_{rs}$ $+ \frac{1}{2} \sum_{pr \in B} \sum_{qs \in A} g_{pqrs} E_{pq} E_{rs}$	$E_{tu}E_{vw} \Psi^{0}\rangle$ $\begin{bmatrix} tv \in A, \ uw \in B \\ uw \in A, \ tv \in B \end{bmatrix}$	$\begin{split} \langle \Psi_{\!X} a_l a_k H_X^{\text{eff}} a_t^\dagger a_u^\dagger \Psi_{\!X} \rangle \\ \langle \Psi_{\!X} a_l^\dagger a_k^\dagger H_X^{\text{eff}} a_t a_u \Psi_{\!X} \rangle \end{split}$
4.	$H'_{\mathrm{TT}} = -\sum_{pq \in A} \sum_{rs \in B} g_{psrq}^{t} t_{pq,rs}$	$egin{aligned} t_{tu,vw} \Psi^0 angle \ [tu \in A, \ vw \in B] \end{aligned}$	$\begin{split} \langle \Psi_{X} T_{lk}^{(1,0)} H_{X}^{\mathrm{eff}} T_{tu}^{(1,0)} \Psi_{X} \rangle \\ \langle \Psi_{X} T_{lk}^{(1,1)} H_{X}^{\mathrm{eff}} T_{tu}^{(1,-1)} \Psi_{X} \rangle \\ \langle \Psi_{X} T_{lk}^{(1,-1)} H_{X}^{\mathrm{eff}} T_{tu}^{(1,1)} \Psi_{X} \rangle \end{split}$

"We summarize here the perturbing functions and cost for each of the perturbations. The rightmost column reports the form of the matrix elements of H^0 required to compute each perturbation; estimating these matrix elements on the fragment state is the most expensive part of FragPT2. If done naively by writing out the full fragment Hamiltonians as a contraction between integrals and this could require estimating 4-RDMs for the dispersion, double-charge transfer (2CT) and triplet—triplet (TT) perturbations, and 5-RDMs for the single-charge transfer (1CT) perturbation.

Hamiltonian can be then decomposed as $H_A + H_B + H_{AB}$, with

$$H_X = \sum_{pq \in X} h_{pq} E_{pq} + \frac{1}{2} \sum_{pqrs \in X} g_{pqrs} e_{pqrs}$$

$$\tag{4}$$

(with $X \in \{A, B\}$), that only act nontrivially on a single fragment, and a term

$$H_{AB} = \sum_{pq \in A} \sum_{rs \in B} g'_{pqrs} E_{pq} E_{rs}$$
(5)

(where $g_{pqrs}' = g_{pqrs} - \frac{1}{2}g_{psrq}$), that includes interactions preserving local spin and charge. The term H_{AB} still introduces interfragment correlations; one way to make the fragments completely independent would be to also treat this term perturbatively (this is the choice made in SAPT. However, including an effective mean-field interaction (originating from H_{AB}) in the nonperturbative solution improves the quality of our $|\Psi^0\rangle$.

To construct the effective Hamiltonian $H_X^{\rm eff}$ for each fragment we use a mean-field decoupling approach. We write the excitation operator as its mean added to a variation upon the mean: $E_{pq} = \langle E_{pq} \rangle + \delta E_{pq}$. The mean is just the one-particle reduced density matrix (1-RDM) of one of the fragments, $\gamma_{pq}^X = \langle \Psi_X | E_{pq} | \Psi_X \rangle$. By substituting in eq 5 we obtain

$$\sum_{pq \in A} \sum_{rs \in B} g'_{pqrs} [E_{pq} \gamma_{rs}^B + \gamma_{pq}^A E_{rs} - \gamma_{pq}^A \gamma_{rs}^B + \delta E_{pq} \delta E_{rs}]$$
(6)

The term $\delta E_{pq} \delta E_{rs}$ will necessarily have zero expectation value on the product state eq 3, as $\langle \Psi_X | \delta E_{pq} | \Psi_X \rangle = 0$. Removing this

term (which we will later treat perturbatively) we obtain the mean-field interaction

$$H_{\rm mf} = \sum_{pq \in A} \sum_{rs \in B} g'_{pqrs} [E_{pq} \gamma_{rs}^B + \gamma_{pq}^A E_{rs} - \gamma_{pq}^A \gamma_{rs}^B]$$
(7)

We can finally define H^0 as

$$H^0 = H_A + H_B + H_{\rm mf} (8)$$

where all terms are operators with support on only a single fragment, thus the ground state $|\Psi^0\rangle$ of H^0 is a product state of the form eq 3. All the terms we removed from H to construct H^0 have zero expectation value on $|\Psi^0\rangle$, thus it is the *lowest energy product state that respects the on-fragment symmetries*.

To find $|\Psi^0\rangle$ we minimize $E_0=\langle H^0\rangle$ by self-consistently solving separate ground state problems on each fragment. Consider the decomposition

$$E_0 = E_A + E_B + E_{\rm mf} \tag{9}$$

where $E_X = \langle \Psi_X | H_X | \Psi_X \rangle$ can be evaluated on a single fragment X and $E_{\rm mf} = \sum_{pq \in A} \sum_{rs \in B} g_{pqrs}' \gamma_{pq}^A \gamma_{rs}^B$ is the mean-field interfragment coupling depending on the fragment 1-RDMs. To find $|\Psi_A\rangle$ and $|\Psi_B\rangle$, we iteratively solve for the ground state of the following coupled Hamiltonians:

$$H_A^{\text{eff}} = H_A + \sum_{pq \in A} \sum_{rs \in B} g'_{pqrs} E_{pq} \gamma_{rs}^B$$
(10)

$$H_B^{\text{eff}} = H_B + \sum_{pq \in A} \sum_{rs \in B} g'_{pqrs} \gamma_{pq}^A E_{rs}$$
(11)

thus minimizing all the terms eq 9. We outline the whole procedure in Algorithm 1. Note that this algorithm can be readily generalized to other MC solvers within the fragment that provide access to the state RDMs (e.g., the variational quantum eigensolver, discussed in Section 4.2.

```
Algorithm 1: Fragment embedding

Input: Active space integrals h_{pq}, g_{pqrs}. Fragment-partitioned sets of orbitals: occupied (O_A, O_B), and virtual (V_A, V_B) subspaces. Convergence threshold \tau.

Output: Optimal product state |\Psi^0\rangle = |\Psi_A\rangle |\Psi_B\rangle

Start from a Hartree-Fock state: \gamma_{pq}^B \leftarrow 2\delta_{pq} for p, q \in O_B; \Delta E, E^0 \leftarrow \infty;

while \Delta E > \tau do

|\Psi_A\rangle, E_c^{\text{eff}} \leftarrow ground state of H_c^{\text{eff}} of Eq. (10); \gamma_{pq}^a \leftarrow (\Psi_A|E_{pq}|\Psi_A\rangle, p, q \in A;

|\Psi_B\rangle, E_B^{\text{eff}} \leftarrow ground state of H_B^{\text{eff}} of Eq. (11); \gamma_{sc}^B \leftarrow (\Psi_B|E_{rs}|\Psi_B\rangle, p, q \in B;

E_{\text{mf}} \leftarrow \sum_{pq\in A} \sum_{rs\in B} g_{prs}^s \gamma_{pq}^s \gamma_{rs}^s,
\Delta E \leftarrow E^0 - (E_A^{\text{eff}} + E_B^{\text{eff}} - E_{\text{mf}});
E^0 \leftarrow (E_A^{\text{eff}} + E_B^{\text{eff}} - E_{\text{mf}})

return |\Psi^0\rangle = |\Psi_A\rangle |\Psi_B\rangle
```

2.3. Multireference Perturbation Theory. While the $|\Psi^0\rangle$ retrieved from Algorithm 1 is a solid starting point, it neglects the correlations between the fragments. If the fragments are sufficiently separated, we expect these correlations to be minimal and recoverable by perturbation theory. We propose using second-order perturbation theory to retrieve the correlation energy of these interactions. The interfragment interaction terms can be classified in four categories, based on whether they conserve charge and/or total spin on each fragment: dispersion H'_{disp} (which conserves both charge and spin of the fragments), single-charge transfer H'_{1CT} and double-charge transfer H'_{2CT} (that conserve charge nor spin), and triplet—triplet coupling H'_{TT} (that conserves charge but not local spin). Thus, the complete decomposition of the Hamiltonian reads:

$$H = H^{0} + H'_{\text{disp}} + H'_{1\text{CT}} + H'_{2\text{CT}} + H'_{\text{TT}}$$
(12)

The definition of these terms is given in Table 1 and their derivation is reported in Appendix 1. We will treat the different perturbations in eq 12 one at a time. First notice that for every perturbation in eq 12, the first order energy correction is zero: $E^1 = \langle \Psi^0 | H' | \Psi^0 \rangle = 0$. We will focus solely on the second order correction to the energy.

To proceed, we need to choose a basis of perturbing functions $\{|\Psi_{\mu}\rangle\}$ used to define the first-order correction to the wave function

$$|\Psi^{1}\rangle = \sum_{\mu} C_{\mu} |\Psi_{\mu}\rangle \tag{13}$$

For the exact second order perturbation energy, we should consider all Slater determinants that can be obtained by applying the terms within H to the set of reference determinants. While this full space of perturbing functions is smaller than the complete eigenbasis of H, it is still unpractically large, and approximations need to be introduced. To choose a compact and expressive basis, we look at the perturbation under consideration. Every perturbative Hamiltonian can be expanded in a linear combination of two-body operators:

$$H' = \sum_{\mu \in A} \sum_{\nu \in B} g_{\mu\nu} O_{\mu}^{A} O_{\nu}^{B} \tag{14}$$

where O_{μ}^{X} is either identity or a product of Fermionic operators on fragment X and $g_{\mu\nu}$ are combinations of one- and twoelectron integrals (see Table 1 for their explicit form). Consider the following (nonorthogonal) basis:

$$|\Psi_{\mu\nu}\rangle = O_{\mu}^{A} O_{\nu}^{B} |\Psi^{0}\rangle \tag{15}$$

This partially contracted basis is a natural choice for compactly representing the wave functions that interact with $|\Psi^0\rangle$ through the perturbations in H'.

Following the choice of perturbing functions, we estimate the matrix elements $\langle \Psi_{\mu\nu}|H^0|\Psi_{\kappa\lambda}\rangle$ in this basis. The overlap $\langle \Psi_{\mu\nu}|\Psi_{\kappa\lambda}\rangle$ must also be computed in order to be able to contract with the $g_{\mu\nu}$ to yield $\langle \Psi^0|H'|\Psi_{\mu\nu}\rangle$. To obtain the coefficients $C_{\mu\nu}$ that define the first-order correction to the wave function, we solve the following linear equations:

$$\sum_{\kappa\lambda} \langle \Psi_{\mu\nu} | H^0 - E^0 | \Psi_{\kappa\lambda} \rangle C_{\kappa\lambda} + \langle \Psi_{\mu\nu} | H' | \Psi^0 \rangle = 0$$
(16)

Then the second-order correction to the energy is given by

$$E^{2} = \langle \Psi^{0} | H' | \Psi^{1} \rangle = \sum_{\mu\nu} \langle \Psi^{0} | H' | \Psi_{\mu\nu} \rangle C_{\mu\nu}$$
(17)

The total second-order PT correction can be expressed as the sum of the different perturbations:

$$E^{2} = E_{\text{disp}}^{2} + E_{1\text{CT}}^{2} + E_{2\text{CT}}^{2} + E_{\text{TT}}^{2}$$
 (18)

The procedure is summarized in Algorithm 2.

```
Algorithm 2: FragPT2

Input: Active space integrals and orbital partitioning as in Algorithm 1.

Zeroth-order product state |\Psi^0\rangle = |\Psi_A\rangle |\Psi_B\rangle.

Output: Second-order perturbative corrections: E_{\rm disp}^2, E_{\rm ICT}^2, E_{\rm 2CT}^2 and E_{\rm TT}^2

for H' \in \{H'_{\rm disp}, H'_{\rm 1CT}, H'_{\rm 2CT}, H'_{\rm TT}\} do

Choose perturbing functions as in Eq. (15);

Compute matrix elements (\Psi_{\mu\nu} | H^0 | \Psi_{\kappa\lambda});

Compute matrix elements (\Psi_{\mu\nu} | H' | \Psi^0);

C_{\mu\nu} \leftarrow solution of Eq. (16);

E^2 \leftarrow \sum_{\mu\nu} \langle \Psi^0 | H' | \Psi_{\mu\nu} \rangle C_{\mu\nu}

return E_{\rm disp}^2, E_{\rm 1CT}^2, E_{\rm 2CT}^2 and E_{\rm TT}^2
```

Computing the matrix elements $\langle \Psi_{\mu\nu}|H^0|\Psi_{\kappa\lambda}\rangle$ is the most expensive part of our algorithm. The tensor product form of the zeroth-order wave function significantly reduces the algorithm's cost by allowing the matrices to factorize in the expectation values of operators on the different fragments, that in turn can be expressed as combinations of fragment RDMs. We outline the idea here, and refer the reader to Appendix 2 for the formal derivation for every perturbation:

$$\begin{split} \langle \Psi_{\mu\nu} | H^{0} | \Psi_{\kappa\lambda} \rangle &= \langle \Psi_{A} | O_{\mu}^{A^{\dagger}} H_{A}^{\text{eff}} O_{\kappa}^{A} | \Psi_{A} \rangle \langle \Psi_{B} | O_{\nu}^{B^{\dagger}} O_{\lambda}^{B} | \Psi_{B} \rangle \\ &+ \langle \Psi_{A} | O_{\mu}^{A^{\dagger}} O_{\kappa}^{A} | \Psi_{A} \rangle \langle \Psi_{B} | O_{\nu}^{B^{\dagger}} H_{B}^{\text{eff}} O_{\lambda}^{B} | \Psi_{B} \rangle \\ &+ E_{\text{mf}} \langle \Psi_{A} | O_{\mu}^{A^{\dagger}} O_{\kappa}^{A} | \Psi_{A} \rangle \langle \Psi_{B} | O_{\nu}^{B^{\dagger}} O_{\lambda}^{B} | \Psi_{B} \rangle \end{split} \tag{19}$$

If there are $N_A N_B$ two-body terms in eq 14, the number of matrix elements that one needs to estimate on each fragment is $\frac{1}{2}N_A N_B (N_A N_B + 1)$. However, if the amount of matrix elements becomes too expensive, it is possible to alleviate the cost without sacrificing much accuracy, for example by using a more compact basis of perturbing functions. For a discussion of further reductions of the cost, see Section 4.1.

3. NUMERICAL DEMONSTRATION

In this section we demonstrate our method by applying it to a range of molecular systems that are well-suited targets for bipartite fragmentation. We have chosen three sets of systems. The first system consists of two N2 molecules at a distance of 2.0 Å, with a (close to equilibrium) bond length of 1.2 Å. In contrast to the other structures, we do not need to cut through a covalent bond and can treat each molecule as a separate fragment. We examine the results of our method while stretching the nitrogen bond in one of the fragments; this is known to rapidly increase static correlation in this system and thus is a good benchmark for the multireference method. The second type of systems we consider comprises a set of aromatic dimers, where two aromatic rings of different kinds are connected by a single covalent bond. Cutting through this bond, we investigate the correlation energies of the dimers with respect to the dihedral angle of the ring alignment. These systems exhibit strong correlation whenever the rings are in the same plane and low correlation when the rings are perpendicular to each other: they are thereby suitable to benchmark both regimes. The final system is butadiene, as the simplest example of the class of polyene molecules that are much studied as 1-D model systems^{51,52} as well as for their importance in various applications.⁵³ -55 Here we cut through the single covalent bond between the middle carbons and investigate the correlation energy with respect to the stretching of the double bonds in a single fragment. This system, albeit slightly artificial, is intriguing due to the significant static correlation within the fragments induced by the dissociating bonds, coupled with substantial dynamic interfragment correlation.

3.1. Numerical Simulation Details. We construct the localized orbitals using a localization scheme implemented in the ROSE code. 56 The FragPT2 method is implemented completely inside the quantum chemical open-source software package PySCF.⁵⁷ Algorithm 1 uses the FCI solver of the program to get the optimal product state of the fragments. The matrix elements in eq 19 by exploiting the software capabilities to manipulate CI-vectors and estimate higher order RDMs. Finally we implemented Algorithm 2 that solves eqs 16,17 for every perturbation in eq 12. To assess the accuracy of our algorithm, we compare the fragment embedding energy E^0 (from Algorithm 1), the FragPT2 energy $E^0 + E^2$ including the perturbative correction (from Algorithm 2), and the exact ground state energy Eexact of the Hamiltonian in eq 1 (calculated with CASCI in a full-molecule active space of double size). The N₂ dimer and aromatic dimer calculations are done in a cc-pVDZ basis set, while butadiene is treated in a 6-31G basis.

3.2. N_2 **Dimer.** As an initial test system, we consider a dimer of nitrogen molecules, i.e., N_2-N_2 . To increase the static correlation within the fragment, we dissociate one of the nitrogen molecules. This bond breaking is modeled using three occupied and three virtual localized orbitals in the active space, representing the σ bond and the two π bonds. This results in an active space of six electrons in six orbitals for each fragment. The results in Figure 2 clearly demonstrate the failure of the Hartree–Fock method due to the high degree of correlation within the fragment. Our multireference solver within the localized active spaces successfully addresses this issue, with E^0 providing a good description of the ground state. There is

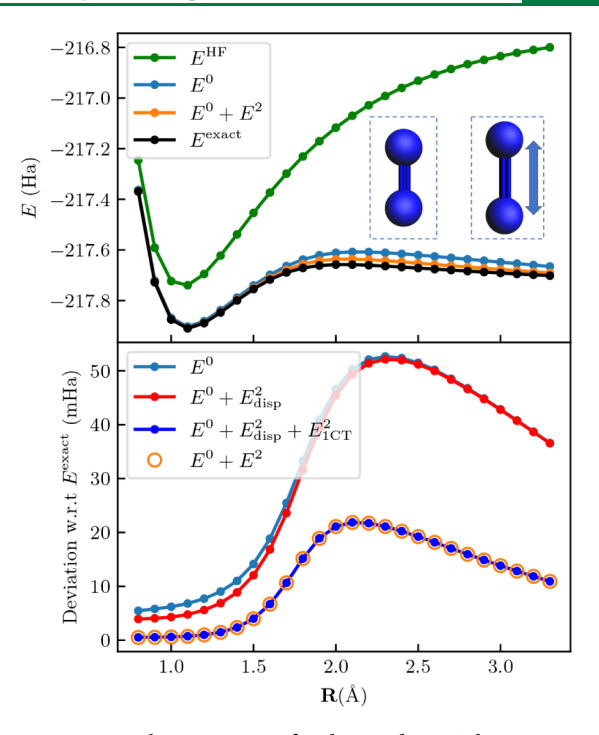


Figure 2. Potential energy curve for the N2 dimer. The upper panel shows a comparison of the curves obtained through Hartree-Fock (E^{HF}), fragment embedding (E^{0}), FragPT2 ($E^{0} + E^{2}$), and fullmolecule CASCI (exact). The two N₂ are parallel and at a distance of 2 Å, and the bond distance of the right dimer is varied. The fragment active spaces each comprise six electrons in six spatial orbitals, corresponding to the triple bonding and antibonding orbitals. Hartree-Fock performs poorly due to the strong intrafragment correlation. The fragment embedding energy E^0 captures the correct behavior of the system, while E^2 gives an additional, small correction in the direction of the exact solution. The bottom panel reports the deviation w.r.t. the exact result over the potential energy curve, where we sequentially add the different perturbative corrections described in Table 1. We first add the dispersion correction E_{disp}^2 (red line) and then the single-charge transfer contribution $E_{\rm 1CT}^2$ (blue line), showing the other contributions are zero by plotting the full FragPT2 energy $E^0 + E^2$ (orange dots).

some minor interfragment correlation, and our perturbative correction brings us closer to the exact solution.

Our data further shows that the perturbative correction arises mainly from the single-charge transfer contribution. Notably, the double-charge transfer and triplet—triplet coupling are zero everywhere. Additionally, we find that for stretched bond lengths, the dispersion interaction between the fragments is minimal. The ability to identify the character of the relevant interactions between fragments is a further advantage of our method.

3.3. Aromatic Dimers. Here we focus on aromatic dimers, i.e., molecules with two aromatic rings that are attached by a single covalent bond. The simplest such system considered is two phenyl rings, known as biphenyl, shown in Figure 1. As the biphenyl case is highly symmetric, other similar molecules can be generated by substituting various ligands for one of the hydrogen atoms, or a nitrogen for a carbon in the phenyl rings. In this manner, we generate a comprehensive benchmark on a variety of systems. Our set of examples is motivated from the different classes of biaryl systems studied by Sanfeliciano et al. in the context of drug design. ⁵⁸

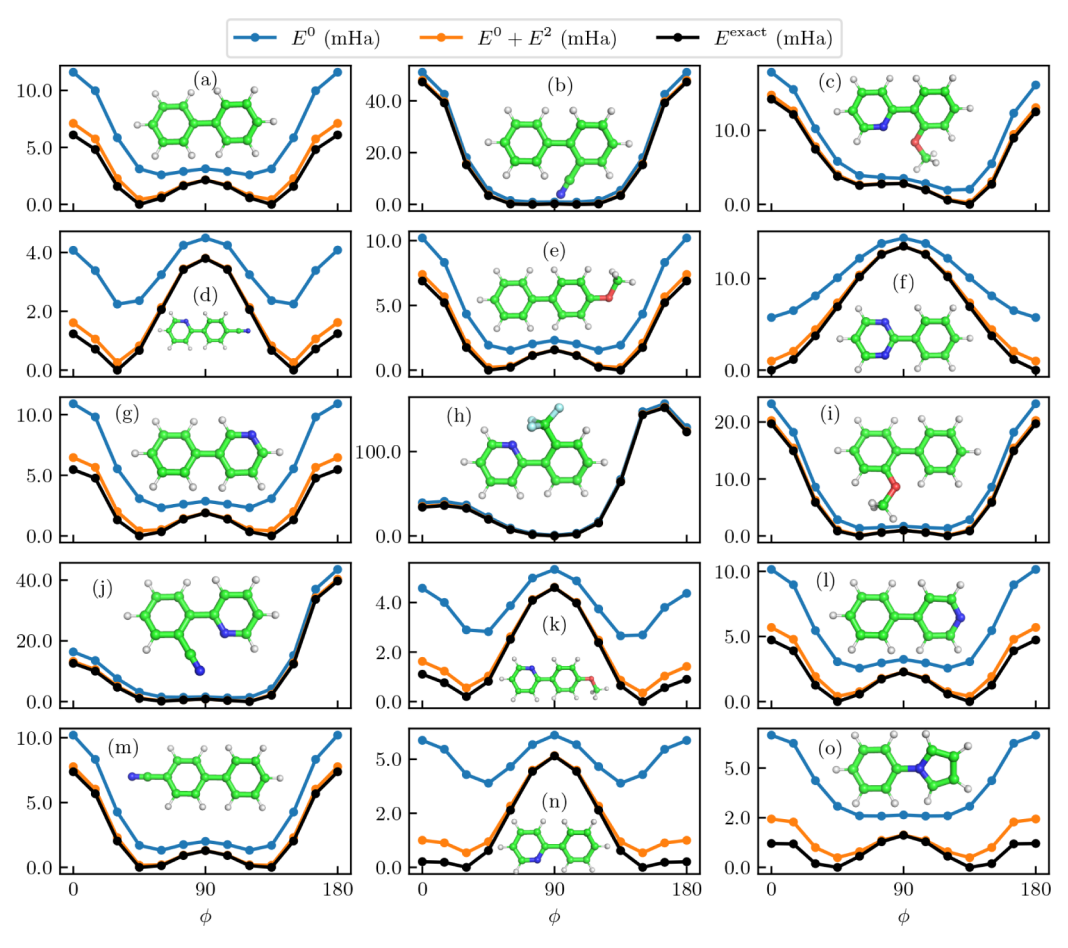


Figure 3. Relative potential energy curves for the set of aromatic dimers, where we vary the dihedral angle ϕ of the two dimers. The molecular orbitals are localized on the fragments naturally defined by the two aromatic rings (including the respective ligands). In principle, for each dimer, we select the active space of six electrons in six orbitals on each fragment that comprise the conjugated $\pi - \pi^*$ system (with some exceptions elaborated on in Section 3.3). Thus, our method cuts down the space for the exact calculation (12 electrons in 12 orbitals) into half. This is small enough to verify our method against an exact CASCI calculation. The blue line represents the fragment embedding energy E^0 . The orange line includes the second-order perturbation energy for all considered perturbations, representing the FragPT2 energy $E^0 + E^2$. The black line reports the exact calculation E^{exact} . All reported energies are relative to the minimum of E^{exact} . The considered molecules are, in row-first order: (a) biphenyl, (b) 2-cyanobiphenyl, (c) 2-(2-methoxyphenyl)pyridine, (d) 2-(4-cyanophenyl)pyridine, (e) 4-methoxybiphenyl, (f) 2-phenylpyrimidine, (g) 3-phenylpyridine, (h) 2-(2-trifluoromethylphenyl)pyridine, (i) 2-methoxybiphenyl, (j) 2-(2-cyanophenyl)pyridine, (k) 2-(4-methoxyphenyl)pyridine, (l) 4-phenylpyridine, (m) 4-cyanobiphenyl, (n) 2-phenylpyridine, and (o) N-phenylpyrrole.

To construct the fragment active spaces, we consider the conjugated $\pi-\pi^*$ system on each ring, typically resulting in six electrons distributed across six orbitals for each fragment. There are a few exceptions to this rule. For pyrrole rings, the relevant aromatic orbitals comprise six electrons in five orbitals. Furthermore, for rings that include a CN or OCH3 substituent (i.e., (c-f), (i-k) and (m) in Figure 3), there is a low-lying π orbital and high-lying π^* orbital that mix with a p orbital of the substituent. These orbitals are excluded from the active space of these fragments, reducing the active space to four electrons in four orbitals. This only provides additional insight into the performance of our method with asymmetric active space sizes in the fragments.

For each dimer, we vary the dihedral angle ϕ of the two planes spanned by the rings, thus rotating over the covalent bond. This gives a potential energy curve with a high variance of correlation energy: if the rings are perpendicular, the aromatic systems are localized and the correlation between the fragments is low. Instead, if the rings are aligned, we expect to see a high amount of correlation between the fragments, and

thus a breakdown of the description of E^0 . The results of our method compared to the exact energies are given in Figure 3.

Our data shows that, for each of the molecules and values of ϕ , E^0 recovers at least 93% of the correlation energy (with an average of 97%). While this is high in absolute terms, the shape of the potential energy curves for these models can be qualitatively wrong. As expected, a product state is not a good approximation if the rings are aligned, as the aromatic system will be delocalized over the molecule. This causes the interactions between the fragments to play a more significant role. The product state is on the other hand a good approximation when the rings are perpendicular, there pushing E⁰ to 99% of the correlation energy. This causes an imbalance between the two configurations and calls for the need to treat the interactions. When we compute the second-order perturbation energy E^2 , it is shown in Figure 3 that sometimes E^0 finds a different minimum than the exact state. In these cases especially, the perturbative corrections need to be calculated to give a more correct shape of the potential energy curve. In Figure 4, one can see that the division of the

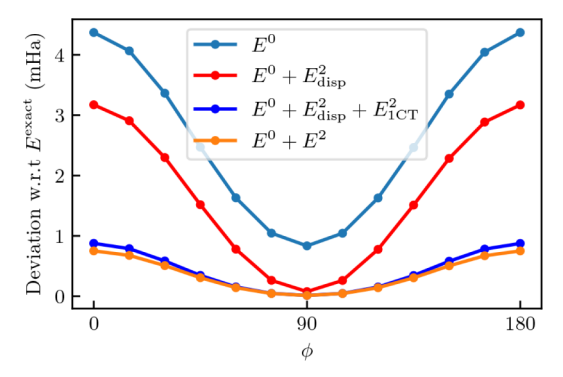


Figure 4. Average errors for the aromatic dimer set. Mean deviation in total energy with respect to the exact result for the complete set of aromatic dimers shown in Figure 3, where we vary the dihedral angle ϕ of the two aromatic rings. We show the result of sequentially adding the different perturbative corrections described in Table 1. The top curve represents the error of fragment embedding energy E^0 . We first add the dispersion correction $E^2_{\rm disp}$, which is giving a constant shift along the dihedral angle. Then, the (single) charge transfer correction $E^2_{\rm 1CT}$ crucially corrects for the behavior where the rings are aligned. Finally, we add the double-charge transfer term $E^2_{\rm 2CT}$ and triplet-triplet term $E^2_{\rm TT}$ together, recovering the final FragPT2 energy $E^0 + E^2$. These last terms contribute an additional small shift to the aligned rings configuration.

perturbation energies can be very constructive in determining the important contributions of the system in question. In case of aromatic dimers, two interactions are important: dispersion and single-charge transfer. While the former takes care of a constant shift over the dihedral angles, the latter is much larger when the aromatic rings are aligned, thus crucial in retrieving the right behavior of PES. The double-charge transfer and triplet—triplet spin exchange terms are not important in these class of molecules.

3.4. Butadiene. Butadiene (C_4H_6) is the final test system that we consider. We define the two fragments by cutting through the middle bond of the molecule. We study the energy of the system while stretch the double bond onto dissociation inside one of the fragments, thereby testing our method to increasing amounts of static correlation inside the fragment. Dissociating the bond additionally causes the leftover molecule to be a radical, thus increasing significantly the strength of the interaction between the fragments.

We define the active spaces by taking the $\pi - \pi^*$ and $\sigma - \sigma^*$ system of the double bonds of both fragments. This results in an active space of four electrons in four orbitals for each fragment.

The potential energy curves are shown in the upper panel of Figure 5. It can be clearly seen that the multireference product state is a correct description at the equilibrium geometry, but its performance is somewhere in between the Hartree–Fock and the exact solution at dissociation. To improve on it, we clearly need the perturbative corrections.

If we analyze the contributions to the perturbative correction plotted in the lower panel of Figure 5, we see that $H'_{1\text{CT}}$ interaction is the most important (contributing around $80 \sim 88\%$ to E^2). Notably, in this system the H'_{TT} contribution is large as well (contributing around $8 \sim 12\%$ to E^2). This is in line with chemical intuition, as this system has low-lying triplet states; 59 a singlet-coupled double triplet excitation may

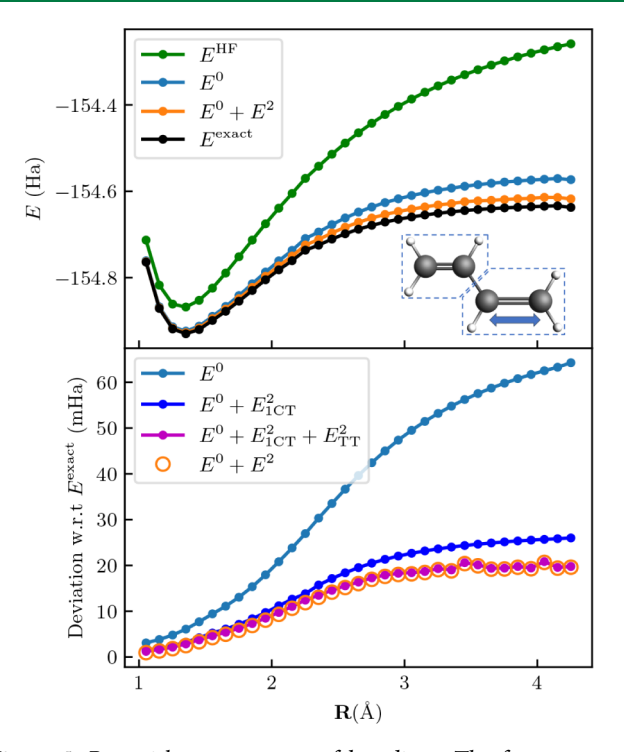


Figure 5. Potential energy curves of butadiene. The fragments are chosen by cutting through the middle bond and subsequently stretching the double bond of one of the fragments, as illustrated in the inset. The curves are color coded like in Figure 2 and show that both intrafragment and interfragment correlations are important to recover the correct behavior. In particular, interfragment correlations are explained by the vicinity of the two fragments and by the radical that is left over after dissociation of the stretched bond. In the lower panel, we show once more the result of sequentially adding the different perturbative corrections described in Table 1. We first add the single-charge transfer contribution $E_{\rm 1CT}^2$ (blue line) and then the triplet—triplet coupling $E_{\rm TT}^2$ (purple line), showing the other contributions are zero by plotting the full FragPT2 energy $E^0 + E^2$ (orange dots).

therefore contribute significantly to the ground state wave function. Again, the ability to separately analyze the different classes of interfragment interactions is useful here, as it allows to consider the correlation in polyenes in terms of products of local excitations.

4. OUTLOOK

4.1. Computational Efficiency. In order to estimate the perturbative corrections in Table 1 we have to construct highorder k-RDMs for all $k \le 5$. These RDMs are tensors with up to 10 indices: constructing and storing them explicitly is computationally expensive. Several methods to evaluate and store high order RDMs in a compressed form have been proposed in the context of e.g., NEVPT2 theory. Resolution of identity (RI), 62 cumulant expansions, 63 tensor contraction with integrals 64,65 are some of the ways to circumvent this bottleneck. Future research should consider how these methods can be applied in the specific case of FragPT2.

To further improve the efficiency of FragPT2, we can consider modifications to the part our algorithm that calculates the perturbative corrections. For example, to circumvent the need to calculate all the different elements of the RDMs, we can compress the basis of perturbing functions in eq 15. One

option is to set the coefficients C_{μ} of eq 13 by the integrals of the perturbation H' under consideration. This gives a single (unnormalized) perturbing function $|\Psi^1\rangle = H'|\Psi^0\rangle$, known in literature as a *strongly contracted basis*. This strongly contracted form has applied with some success in the context of NEVPT2.³⁸ The bottleneck of the algorithm then becomes estimating higher order powers of the Hamiltonian and the perturbations on $|\Psi^0\rangle$, effectively equivalent to the first order of a moment expansion.^{38,66} Another possible approach to reducing the cost of computing perturbations relies on stochastic formulations of MRPT, which have also been studied in the context of strongly contracted NEVPT2.^{67–69} In these approaches, the necessary quantities were determined in a quantum Monte Carlo (QMC) framework.

4.2. Integration with Quantum Algorithms. In this manuscript, we focused on solving the single fragments with FCI, but our framework is compatible with any method that can recover RDMs of fragment wave functions. Quantum algorithms have emerged as promising tools for tackling classically hard electronic structure problems, but they come with specific limitations distinct from those of classical algorithms. Fragmentation and embedding techniques are critical for defining tasks suited to quantum algorithms, enabling a focus on strongly correlated active sites while reducing problem sizes. Recent studies have explored integrating quantum algorithms into embedding schemes, including SAPT (for both near-term variational 70,71 and faulttolerant⁷² approaches) and LASSCF. 47,73 In this context, we discuss integrating FragPT2 with the variational quantum eigensolver (VQE).74,75

The VQE prescribes to prepare on a quantum device an ansatz state $|\Psi(\theta)\rangle$, as a function of a set of classical parameters θ which are then optimized to minimize the state energy $E(\theta) = \langle \Psi(\theta)|H|\Psi(\theta)\rangle$. Having access to a quantum device allows to produce states which can be hard to represent on a classical computer, enabling the implementation of ansätze such as unitary coupled cluster and other heuristic constructions however, sampling the energy and other properties from the quantum state incurs a large sampling cost, which is worsened by the required optimization overhead.

Integrating FragPT2 with the VQE is straightforward. For each fragment X, a separate parametrized wave function $|\Psi_X(\theta_X)\rangle$ is represented, reconstructing an ansatz $|\Psi_A(\theta_A)\rangle|\Psi_A(\theta_B)\rangle$ for the product state eq 3. As no quantum correlation is needed, multiple wave functions can be prepared in parallel in separate quantum devices, or even serially on the same device; this can allow to treat larger chemical systems with limited-size quantum devices. We can find the lowest-energy product state directly by minimizing the expectation value of the Hamiltonian

$$E(\theta_A, \theta_B) = \langle \Psi_A(\theta_A) | \langle \Psi_B(\theta_B) | H | \Psi_A(\theta_A) \rangle | \Psi_B(\theta_B) \rangle \tag{20}$$

this energy can be estimated by measuring the one- and two-body reduced density matrices separately on each fragment. As shown in Section 2.2, the minimum energy product state matches the solution of the mean field embedding.

Integrating VQE with fragmentation techniques can help describe binding energies, proposed in literature with a method based on symmetry adapted perturbation theory and termed SAPT(VQE). SAPT(VQE) addresses the same terms as Algorithm 1, but uses a perturbative expansion instead of mean-field coupling for terms dependent on fragment 1- and 2-

RDMs. It employs two nonorthogonal orbital sets for the fragments, limiting this method to noncovalently bonded fragments. Inspired by SAPT(VQE), Algorithm 1 could be adapted to measure interaction energies. A thorough comparison of the two methods and studying their dependence on molecular orbitals and atomic basis set is a promising area for future work. SAPT has also recently been applied to fault-tolerant quantum algorithms, overcoming some of the limitations of near-term devices.⁷²

As per Algorithm 2, to recover the perturbative corrections accounting for interfragment interactions we need to extract higher-order reduced density matrices from each fragment's wave function. Perturbation theory for the variational quantum eigensolver has been studied in the context of recovering dynamical correlations. ^{80,81} Using measurement optimization techniques from refs. 82 and 83, estimating all the elements of the k-RDMs on a fragment active space of N orbitals to a precision ϵ requires $O(\epsilon^{-2}N^k)$ samples. In practice this makes naively estimating the perturbative corrections very costly, especially for the single-charge transfer terms H'_{1CT} that require 5-RDMs (see Table 1). An interesting direction for future research might consider using shadow tomography and its Fermionic extension ^{84,85} to estimate RDMs to all orders at the same time.

4.3. Further Extensions. Extension to multiple fragments — This paper focused on the case of two active fragments. However, it is relatively straightforwardly applied to more. The lowest energy product state can be retrieved by trivially extending the algorithm, looping through the fragments and solving exactly the active fragment feeling the mean-field of the inactive fragments, until reaching convergence. Subsequently, we can treat the interfragment interactions that can span four fragments at a time at most (as the Hamiltonian is a two-body operator), which is a coupled charge transfer excitation. While the perturbing functions then have to be extended to these types of excitations, the matrix elements that one has to estimate will factorize in the same way, and the algorithm will not be more costly than for two fragments (i.e., no higher order RDMs will have to be estimated). Working out the exact expressions and implementing a truly many-fragment algorithm is part of future work.

Localized orbitals beyond Hartree-Fock — The Hartree-Fock determinant is known to be an unstable reference in dissociating systems and other highly correlated molecules.^{86,87} To generate the input orbitals, one might want to change from a cheap mean-field method to a slightly more expensive CASSCF calculation with a small active space. As the localization scheme can handle any input orbitals, our method can be trivially adapted to a better choice of reference orbitals that already takes into account some correlation. Additionally, one can include intrafragment orbital-optimization during the fragment embedding (Algorithm 1). A simple approach would involve using a CASSCF solver on the individual fragments, with orbital rotations constrained to each fragment to keep the fragments separated. This could enhance the method's accuracy and provide a better starting point for perturbation theory. In this spirit, a version LASSCF³³ or vLASSCF³⁴ could be recovered as an extension of our method where orbital rotations between fragment active spaces are also allowed and optimized self-consistently.

NEVPT2-like perturbations—So far we have treated the interactions only inside the complete active space, i.e., our H

from eq 1 involves indices within either active fragment. To retrieve more of the dynamical correlation energy, the core idea of NEVPT2 is to include excitations involving also the inactive orbitals in a perturbative way. We can build on top of our previous approach by including additional perturbations and perturbing functions. Correspondingly, we can augment our Hamiltonian from eq 1 as,

$$H = H^0 + H'_{\text{act}} + H'_{\text{inact}} \tag{21}$$

where $H_{\rm inact}'$ consists of the various classes of perturbations involving excitations from the core to the active space, the active space to the virtual space and the core to the active space. For the form of these perturbations, see ref. 38 . It is straightforward to extend the methods from NEVPT2 to the case of multiple active fragments, and again the matrix elements will factorize on different fragments in the same way, relieving the need to estimate additional matrix elements on the multireference fragment solvers.

5. CONCLUSION

In this work, we introduced a novel multireference multifragment embedding framework called FragPT2. We showed that our method gives accurate results for a reduced cost in active space size, especially when the fragments are well-separated. Our comprehensive numerical benchmarks on a variety of molecules show that 1. Intrafragment static correlation can be retrieved by an MC product state ansatz (E^0) 2. Interfragment correlation can be treated as a perturbative correction (E^2) 3. A combination of these is needed to recover the correct shape of the potential energy curve. Using a decomposition of the Hamiltonian based on fragment symmetries, we can distinguish the contributions to the interfragment correlation in E^2 , providing insight into important interactions within the studied systems. Furthermore, our adapted localization scheme allows to define molecular fragments that cut through covalent bonds. In this case, perturbative corrections describing interfragment charge transfer (and, to a lesser extent, triplet-triplet spin exchange) are crucial for accurately describing the system. Future research directions include improving the efficiency of high-order RDM estimation, integrating FragPT2 with variational quantum algorithms, and extensions to multiple fragments for broader applicability.

Our multireference embedding scheme could find broad applications, for instance in understanding the spatial dependence of the correlation energy in π -stacked systems and other biochemically important systems, ⁸⁸ modeling supramolecular complex formation ⁸⁹ in metal ion separation, or in analyzing metallophilic interactions.

APPENDIX A

A. Hamiltonian decomposition

In this appendix, we give a detailed derivation of the terms in the decomposition eq 2 of the full active-space molecular Hamiltonian.

We start from the full Hamiltonian eq 1, and we rewrite the quartic excitation operators $e_{pqrs}=E_{pq}E_{rs}-\delta_{qr}E_{ps}$ in terms of the quadratic E_{pqr} obtaining

$$H = \sum_{pq} h_{pq} E_{pq} - \frac{1}{2} \sum_{pq} \sum_{r} g_{prrq} E_{pq} + \frac{1}{2} \sum_{pqrs} g_{pqrs} E_{pq} E_{rs}$$
(22)

We will separately deal with the terms that conserve charge on each fragment (in Appendix A.1) and those that transfer charge between fragments (in Appendix A.2). It can be easily identified whether a term preserves charge on each fragment by counting the number of electrons moved across orbitals, as all orbitals $\{p, q, r, s\}$ pertain to either fragment A or B.

A.1. Charge-conserving terms. In this section we derive the charge-conserving interfragment terms $H'_{\rm disp}$ and $H'_{\rm TT}$, as well as the on-fragment Hamiltonians H_A and H_B .

The one-body term of eq 22 only conserves charge if p and q are both in the A fragment or both in the B fragment, these terms will respectively be part of H_A and H_B . The two-body term of eq. 22 includes terms where all p, q, r, s are part of the same fragment: these will also be part of H_A and H_B .

The other possible options that preserve charge while including terms on both fragments are

$$\frac{1}{2} \sum_{pq \in A} \sum_{rs \in B} g_{pqrs} E_{pq} E_{rs} + \frac{1}{2} \sum_{pq \in B} \sum_{rs \in A} g_{pqrs} E_{pq} E_{rs}
+ \frac{1}{2} \sum_{pq \in A} \sum_{rs \in B} g_{psrq} E_{ps} E_{rq} + \frac{1}{2} \sum_{rs \in B} \sum_{pq \in A} g_{rqps} E_{rq} E_{ps} \tag{23}$$

It is straightforward to show that the first two terms are equivalent by using the symmetry $g_{pqrs} = g_{rspq}$ and the excitation operator commutation relations $[E_{pq}, E_{rs}] = E_{ps}\delta_{qr} - E_{rq}\delta_{ps}$. These terms represent the Coulomb interactions between the fragments. The latter two terms describe the exchange interactions between the fragments.

We rewrite the exchange term using Fermionic commutation rules—using the notation p_X being an orbital index on fragment X we get

$$\begin{split} E_{p_{A}s_{B}}E_{r_{B}q_{A}} &= \sum_{\sigma\tau} a^{\dagger}_{p_{A}\sigma}a_{s_{B}\sigma}a^{\dagger}_{r_{B}\tau}a_{q_{A}\tau} \\ &= \sum_{\sigma\tau} \left(\delta_{r_{B}s_{B}}\delta_{\sigma\tau}a^{\dagger}_{p_{A}\sigma}a_{q_{A}\tau} - a^{\dagger}_{p_{A}\sigma}a_{q_{A}\tau}a^{\dagger}_{r_{B}\tau}a_{s_{B}\sigma} \right) \\ &= \delta_{r_{B}s_{B}}E_{p_{A}q_{A}} - a^{\dagger}_{p_{A}}a_{q_{A}}a^{\dagger}_{r_{B}\sigma}a_{s_{B}\alpha} - a^{\dagger}_{p_{A}}a_{q_{A}}\beta^{\dagger}_{r_{B}\beta}a_{s_{B}\beta} \\ &- a^{\dagger}_{p_{A}\alpha}a_{q_{A}\beta}a^{\dagger}_{r_{B}\beta}a_{s_{B}\alpha} - a^{\dagger}_{p_{A}\beta}a_{q_{A}\alpha}a^{\dagger}_{r_{B}\alpha}a_{s_{B}\beta} \\ &= \delta_{r_{B}s_{B}}E_{p_{A}q_{A}} - S^{0,0}_{p_{A}q_{A}}S^{0,0}_{r_{B}s_{B}} - T^{1,0}_{p_{A}q_{A}}T^{1,0}_{r_{B}s_{B}} + T^{1,1}_{p_{A}q_{A}}T^{1,-1}_{r_{B}s_{B}} \\ &+ T^{1,-1}_{p_{A}q_{A}}T^{1,1}_{r_{B}s_{B}} \end{split}$$

where we use the definition of the spin operators:⁸⁶

$$S_{p_X q_X}^{(0,0)} = \frac{1}{\sqrt{2}} E_{p_X q_X} = \frac{1}{\sqrt{2}} (a_{p_X \alpha}^{\dagger} a_{q_X \alpha} + a_{p_X \beta}^{\dagger} a_{q_X \beta})$$
 (25)

$$T_{p_{\chi}q_{\chi}}^{(1,0)} = \frac{1}{\sqrt{2}} (a_{p_{\chi}\alpha}^{\dagger} a_{q_{\chi}\alpha} - a_{p_{\chi}\beta}^{\dagger} a_{q_{\chi}\beta})$$
 (26)

$$T_{p_X q_X}^{(1,1)} = -a_{p_X \alpha}^{\dagger} a_{q_X \beta} \tag{27}$$

$$T_{p_X q_X}^{(1,-1)} = a_{p_X \rho}^{\dagger} a_{q_X \alpha} \tag{28}$$

and

$$a_{p\alpha}^{\dagger} a_{q\alpha} = \frac{1}{\sqrt{2}} (S_{pq}^{(0,0)} + T_{pq}^{(1,0)})$$

$$a_{p\beta}^{\dagger} a_{q\beta} = \frac{1}{\sqrt{2}} (S_{pq}^{(0,0)} - T_{pq}^{(1,0)})$$
(29)

Notice that the last three terms of eq 24 conserve the total spin of the system, but flip the local spin of the individual fragments. Separating out these terms from the expansion of eq. 23 we obtain the triplet—triplet interaction Hamiltonian:

$$\begin{split} H_{\mathrm{TT}}' &= \sum_{pq \in A} \sum_{rs \in B} g_{psrq} T_{p_{A}q_{A}}^{1,0} T_{r_{B}s_{B}}^{1,0} + T_{p_{A}q_{A}}^{1,1} T_{r_{B}s_{B}}^{1,-1} + T_{p_{A}q_{A}}^{1,-1} T_{r_{B}s_{B}}^{1,1} \\ &= -\sum_{pq \in A} \sum_{rs \in B} g_{psrq} t_{pq,rs} \end{split} \tag{30}$$

where
$$t_{pq,rs} = T_{pq}^{1,0} T_{rs}^{1,0} - T_{pq}^{1,1} T_{rs}^{1,-1} - T_{pq}^{1,-1} T_{rs}^{1,1}$$
.

After subtracting this term from eq 23, we arrive at the following expression for the Hamiltonian that includes all fragment charge-conserving and spin-conserving terms: $H_A + H_B + H_{AB}$, which can be easily split in the three terms

$$H_{A} = \sum_{pq \in A} h_{pq} E_{pq} - \frac{1}{2} \sum_{pqr \in A} g_{prrq} E_{pq} + \sum_{pqrs \in A} g_{pqrs} E_{pq} E_{rs}$$
(31)

$$H_{B} = \sum_{pq \in B} h_{pq} E_{pq} - \frac{1}{2} \sum_{pqr \in B} g_{prrq} E_{pq} + \sum_{pqrs \in B} g_{pqrs} E_{pq} E_{rs}$$
(32)

$$H_{\rm mf} + H_{\rm disp}' = \sum_{pq \in A} \sum_{rs \in B} \left[g_{pqrs} - \frac{1}{2} g_{psrq} \right] E_{pq} E_{rs}$$
(33)

where the last row can be further split in a mean-field interaction term $H_{\rm mf}$ and a dispersion term $H'_{\rm disp}$: the mean-field interaction is defined self-consistently on the basis of the solution of the Hamiltonian $H^0 = H_A + H_B + H_{\rm mf}$, as we showed in Section 2.2.

A.2. Charge transfer terms. We now work on separating the terms that involve charge transfers between the fragments. As the molecular Hamiltonian contains only one-body and two-body terms, we only need to consider single-charge and double-charge transfers, respectively classified as part of H'_{1CT} and H'_{2CT} .

We first isolate the single-charge transfer terms. These include the single-body terms of eq 22 where p and q pertain to different fragments:

$$\sum_{p \in A} \sum_{q \in B} h_{pq} E_{pq} + \sum_{p \in B} \sum_{q \in A} h_{pq} E_{pq}$$
(34)

along with the two-body terms where three indices pertain to a fragment and one pertains to the other:

$$\frac{1}{2} \left[\sum_{pqr \in A} \sum_{s \in B} + \sum_{pqs \in A} \sum_{r \in B} + \sum_{prs \in A} \sum_{q \in B} + \sum_{qrs \in A} \sum_{p \in B} \right] \\
\left(g_{pqrs} (E_{pq} E_{rs} - \delta_{qr} E_{ps}) \right) \\
+ \frac{1}{2} \left[\sum_{pqr \in B} \sum_{s \in A} + \sum_{pqs \in B} \sum_{r \in A} + \sum_{prs \in B} \sum_{q \in A} + \sum_{qrs \in B} \sum_{p \in A} \right] \\
\left(g_{pqrs} (E_{pq} E_{rs} - \delta_{qr} E_{ps}) \right) \tag{35}$$

where for brevity we write multiple sums (in brackets) sharing the same summand (in parentheses). We can simplify this using the symmetries of the two-body integral $g_{pqrs}=g_{rspq}=g_{qprs}=g_{pqsr}$ and the commutation relations of excitation operators $[E_{pq},E_{rs}]=E_{ps}\delta_{qr}-E_{rq}\delta_{ps}$, obtaining

$$-\sum_{p \in A} \sum_{q \in B} \left[\sum_{r \in A} g_{prrq} \right] E_{pq} - \sum_{p \in B} \sum_{q \in A} \left(\sum_{r \in B} g_{prrq} \right) E_{pq}$$

$$+ \sum_{pqr \in A} \sum_{s \in B} g_{pqrs} E_{pq} (E_{rs} + E_{sr})$$

$$+ \sum_{pqr \in B} \sum_{s \in A} g_{pqrs} E_{pq} (E_{rs} + E_{sr})$$
(36)

Combining this with the one-body term eq 34 we define the single-charge transfer term

$$H'_{1CT} = \sum_{p \in A} \sum_{q \in B} \left[h_{pq} - \sum_{r \in A} g_{prrq} \right] E_{pq}$$

$$+ \sum_{p \in B} \sum_{q \in A} \left[h_{pq} - \sum_{r \in B} g_{prrq} \right] E_{pq}$$

$$+ \sum_{pqr \in A} \sum_{s \in B} g_{pqrs} E_{pq} [E_{rs} + E_{sr}]$$

$$+ \sum_{pqr \in B} \sum_{s \in A} g_{pqrs} E_{pq} [E_{rs} + E_{sr}]$$
(37)

The double-charge transfer is simpler, as there are just two two-body terms that allow for a double-charge transfer:

$$H'_{2\text{CT}} = \frac{1}{2} \sum_{pr \in A} \sum_{qs \in B} g_{pqrs} E_{pq} E_{rs} + \frac{1}{2} \sum_{pr \in B} \sum_{qs \in A} g_{pqrs} E_{pq} E_{rs}$$
(38)

One can easily verify that

$$H = H_{A} + H_{B} + H_{\rm mf} + H_{\rm disp}' + H_{\rm TT}' + H_{\rm 1CT}' + H_{\rm 2CT}'$$

APPENDIX B

B. Fragment matrix elements

This section contains derivations of the expressions for the zeroth-order Hamiltonian matrix elements $\langle \Psi_{\mu\nu}|H^0|\Psi_{\kappa\lambda}\rangle$ for every perturbation $H'=\sum_{\mu\nu}g_{\mu\nu}O^A_\mu O^B_\nu$. We will focus here on estimating these matrix elements exactly without any approximation, resulting in the need for higher order RDMs. For a discussion of future work to improve efficiency, see Section 4.1. In general, the expressions are given as

$$\begin{split} \langle \Psi_{\mu\nu} | H^0 | \Psi_{\kappa\lambda} \rangle &= \langle \Psi_A | O_\mu^{A^\dagger} H_A^{\text{eff}} O_\kappa^A | \Psi_A \rangle \langle \Psi_B | O_\nu^{B^\dagger} O_\lambda^B | \Psi_B \rangle \\ &+ \langle \Psi_A | O_\mu^{A^\dagger} O_\kappa^A | \Psi_A \rangle \langle \Psi_B | O_\nu^{B^\dagger} H_B^{\text{eff}} O_\lambda^B | \Psi_B \rangle \\ &+ E_{\text{mf}} \langle \Psi_A | O_\mu^{A^\dagger} O_\kappa^A | \Psi_A \rangle \langle \Psi_B | O_\nu^{B^\dagger} O_\lambda^B | \Psi_B \rangle \end{split} \tag{39}$$

$$\langle \Psi^{0}|H'|\Psi_{\kappa\lambda}\rangle = \sum_{\mu\nu} g_{\mu\nu} \langle \Psi_{A}|O_{\mu}^{A\dagger}O_{\kappa}^{A}|\Psi_{A}\rangle \langle \Psi_{B}|O_{\nu}^{B\dagger}O_{\lambda}^{B}|\Psi_{B}\rangle \tag{40}$$

where we defined the perturbing functions as $|\Psi_{\mu\nu}\rangle = O_{\mu}^{A}O_{\nu}^{B}|\Psi_{A}\rangle|\Psi_{B}\rangle$. We have

$$\langle \Psi_{X} | O_{\mu}^{X} H_{X}^{\text{eff}} O_{\nu}^{X} | \Psi_{X} \rangle = \sum_{pq \in X} \left(h_{pq} + \sum_{rs \in Y} g'_{pqrs} \gamma_{rs}^{Y} - \sum_{r \in X} g_{prrq} \right)$$

$$\langle \Psi_{X} | O_{\mu}^{X} E_{pq} O_{\nu}^{X} | \Psi_{X} \rangle + \sum_{pqrs \in X} g_{pqrs} \langle \Psi_{X} | O_{\mu}^{X} E_{pq} E_{rs} O_{\nu}^{X} | \Psi_{X} \rangle$$

$$(41)$$

Thus, the relevant operator matrix elements to estimate are $\langle \Psi_X | O_\mu^X E_{\nu q} E_{rs} O_\nu^X | \Psi_X \rangle$, $\langle \Psi_X | O_\mu^X E_{\nu q} O_\nu^X | \Psi_X \rangle$, and $\langle \Psi_X | O_\mu^X O_\nu^X | \Psi_X \rangle$.

B.1. Dispersion. For the case of the dispersion perturbation, we use the perturbing functions

$$E_{tu}E_{vw}|\Psi^0\rangle[tu\in A, vw\in B] \tag{42}$$

Thus, we straightforwardly identify $O^X_\mu \to E_{pq}$ and the most expensive matrix element to compute is

$$\langle \Psi_X | E_{\nu\nu} E_{pq} E_{rs} E_{tu} | \Psi_X \rangle \tag{43}$$

i.e. a 4-particle reduced density matrix.

B.2. Single-charge transfer. The single-charge transfer case is a bit more complicated. We like to preserve the total spin, so we use the spin-free excitation operators to define the perturbing functions as

$$E_{tu}E_{vw}|\Psi^{0}\rangle \begin{bmatrix} tuv\in A,\ w\in B\\ tuw\in A,\ v\in B\\ tuv\in B,\ w\in A\\ tuw\in B,\ v\in A \end{bmatrix} \tag{44}$$

That means a straightforward decomposition into $O_{\mu}^{A}O_{\nu}^{B}$ is more intricate because of the sum over spin. Instead, we have $\sum_{\sigma}E_{p_{\chi}q_{\chi}}a_{\nu_{\chi}\sigma}^{\dagger}a_{w_{\gamma}\sigma}$ and $\sum_{\sigma}E_{p_{\gamma}q_{\chi}}a_{\nu_{\chi}\sigma}^{\dagger}a_{w_{\gamma}\sigma}$. Let us work out the matrix elements explicitly for the first case in eq 44. This is easily generalizable to the other cases. The total matrix element becomes

$$\begin{split} \langle \Psi_{k_{A}l_{A}m_{A}n_{B}}|H^{0}|\Psi_{t_{A}u_{A}v_{A}w_{B}}\rangle &= \sum_{\sigma\tau} \langle \Psi_{A}|a_{m\sigma}E_{lk}H_{A}^{\text{eff}}E_{tu}a_{v\tau}^{\dagger}|\Psi_{A}\rangle \langle \Psi_{B}|a_{n\sigma}^{\dagger}a_{w\tau}|\Psi_{B}\rangle \\ &+ \sum_{\sigma\tau} \langle \Psi_{A}|a_{m\sigma}E_{lk}E_{tu}a_{v\tau}^{\dagger}|\Psi_{A}\rangle \langle \Psi_{B}|a_{n\sigma}^{\dagger}H_{B}^{\text{eff}}a_{w\tau}|\Psi_{B}\rangle \\ &+ E_{\text{mf}} \sum_{\sigma\tau} \langle \Psi_{A}|a_{m\sigma}E_{lk}E_{tu}a_{v\tau}^{\dagger}|\Psi_{A}\rangle \langle \Psi_{B}|a_{n\sigma}^{\dagger}a_{w\tau}|\Psi_{B}\rangle \end{split} \tag{45}$$

As E_{pq} and $H_X^{\rm eff}$ preserve spin, and $|\Psi_X\rangle$ are eigenfunctions of S^2 , we can replace the double sum over spin by a single one as $\sigma = \tau$. Now substituting $O_\mu^X \to E_{tu} a_{\nu\sigma}^{\dagger}$ in eq 41 the most expensive object to estimate will be

$$\langle \Psi_{X} | a_{m\sigma} E_{lk} E_{pq} E_{rs} E_{tu} a_{v\sigma}^{\dagger} | \Psi_{X} \rangle \tag{46}$$

i.e. a 5-particle reduced density matrix.

B.3. Double-charge transfer. For the double-charge transfer we have the following set of perturbing functions:

$$E_{tu}E_{vw}|\Psi^{0}\rangle\begin{bmatrix}tv\in A,\,uw\in B\\uw\in A,\,tv\in B\end{bmatrix}\tag{47}$$

This makes the total matrix element equal to

$$\begin{split} \langle \Psi_{k_{A}lgm_{A}n_{B}}|H^{0}|\Psi_{t_{A}u_{B}v_{A}w_{B}}\rangle &= \sum_{\sigma\tau\kappa\lambda} \langle \Psi_{A}|a_{m\sigma}a_{k\tau}H_{A}^{\rm eff}a_{t\kappa}^{\dagger}a_{\nu\lambda}^{\dagger}|\Psi_{A}\rangle\langle \Psi_{B}|a_{n\sigma}^{\dagger}a_{l\tau}^{\dagger}a_{u\kappa}a_{w\lambda}|\Psi_{B}\rangle \\ &+ \sum_{\sigma\tau\kappa\lambda} \langle \Psi_{A}|a_{m\sigma}a_{k\tau}a_{t\kappa}^{\dagger}a_{\nu\lambda}^{\dagger}|\Psi_{A}\rangle\langle \Psi_{B}|a_{n\sigma}^{\dagger}a_{l\tau}^{\dagger}H_{B}^{\rm eff}a_{u\kappa}a_{w\lambda}|\Psi_{B}\rangle \\ &+ E_{\rm mf} \sum_{\sigma\tau\kappa\lambda} \langle \Psi_{A}|a_{m\sigma}a_{k\tau}a_{t\kappa}^{\dagger}a_{\nu\lambda}^{\dagger}|\Psi_{A}\rangle\langle \Psi_{B}|a_{n\sigma}^{\dagger}a_{l\tau}^{\dagger}a_{u\kappa}a_{w\lambda}|\Psi_{B}\rangle \end{split} \tag{48}$$

Here there also simplifications possible regarding the sum over spin. Namely, only the following options are nonzero: σ , τ , κ , $\lambda \in \{\alpha\alpha\alpha\alpha$, $\beta\beta\beta\beta$, $\alpha\beta\alpha\beta$, $\alpha\beta\beta\alpha$, $\beta\alpha\alpha\beta$, $\beta\alpha\beta\alpha$. Regardless, making the identification $O^X_\mu \to a^\dagger_{t\sigma}a^\dagger_{v\sigma}$ in eq 41, the most expensive object to estimate is

$$\langle \Psi_{X} | a_{m\sigma} a_{k\tau} E_{pq} E_{rs} a_{t\kappa}^{\dagger} a_{\nu\lambda}^{\dagger} | \Psi_{X} \rangle \tag{49}$$

and similarly for $O^X_\mu \to a_{t\sigma} a_{v\sigma}$, this is as expensive as estimating a 4-particle reduced density matrix.

B.4. Triplet—*triplet*. The triplet—triplet perturbing functions are given by

$$t_{tuvw}|\Psi^0\rangle[tu\in A, vw\in B] \tag{50}$$

where $t_{tuvw}=T_{tu}^{1,0}T_{vw}^{1,0}-T_{tu}^{1,1}T_{vw}^{1,-1}-T_{tu}^{1,-1}T_{vw}^{1,1}$ (see Appendix A.1 for their definition). Observe that, for any fragment operator O^X that preserves spin, all matrix elements $\langle \Psi_X|T^{(1,m')}O^XT^{(1,m')}|\Psi_X\rangle$ are only nonzero if m+m'=0, where $m,m'\in\{-1,0,-1\}$. Thus, we can make the following statement:

$$\begin{split} &\langle \Psi^{0}_{klmn}|O^{A}O^{B}|\Psi^{0}_{tuvw}\rangle = \langle \Psi^{0}|t^{\dagger}_{k_{A}l_{A},m_{B}n_{B}}O^{A}O^{B}t_{t_{A}u_{A},v_{B}w_{B}}|\Psi^{0}\rangle \\ &= \langle \Psi_{A}|T^{(1,0)}_{lk}O^{A}T^{(1,0)}_{tu}|\Psi_{A}\rangle \langle \Psi_{B}|T^{(1,0)}_{nm}O^{B}T^{(1,0)}_{vw}|\Psi_{B}\rangle \\ &+ \langle \Psi_{A}|T^{(1,1)}_{lk}O^{A}T^{(1,-1)}_{tu}|\Psi_{A}\rangle \langle \Psi_{B}|T^{(1,-1)}_{nm}O^{B}T^{(1,1)}_{vw}|\Psi_{B}\rangle \\ &+ \langle \Psi_{A}|T^{(1,-1)}_{lk}O^{A}T^{(1,1)}_{tu}|\Psi_{A}\rangle \langle \Psi_{B}|T^{(1,1)}_{nm}O^{B}T^{(1,-1)}_{vw}|\Psi_{B}\rangle \end{split} \tag{51}$$

Finally, the matrix element of H^0 in this basis is thus equal to

$$\begin{split} \langle \Psi_{k_{A}^{I}_{A}m_{B}n_{B}}|H^{0}|\Psi_{t_{A}u_{A}v_{B}w_{B}}\rangle &= \sum_{m+m'=0} \langle \Psi_{A}|T_{lk}^{(1,m)}H_{A}^{\text{eff}}T_{tu}^{(1,m')}|\Psi_{A}\rangle \langle \Psi_{B}|T_{nm}^{(1,m')}T_{vw}^{(1,m)} \\ |\Psi_{B}\rangle &+ \sum_{m+m'=0} \langle \Psi_{A}|T_{lk}^{(1,m)}T_{tu}^{(1,m')}|\Psi_{A}\rangle \langle \Psi_{B}|T_{nm}^{(1,m')}H_{A}^{\text{eff}}T_{vw}^{(1,m)}|\Psi_{B}\rangle \\ &+ E_{\text{mf}} \sum_{m+m'=0} \langle \Psi_{A}|T_{lk}^{(1,m)}T_{tu}^{(1,m')}|\Psi_{A}\rangle \langle \Psi_{B}|T_{nm}^{(1,m')}T_{vw}^{(1,m')}|\Psi_{B}\rangle \end{split} \tag{52}$$

The most expensive object to estimate in the triplet-triplet case is then, identifying $O_u^X \to T_{tu}^{(1,m)}$ in eq 41:

$$\langle \Psi_{X}|T_{lk}^{(1,m)}E_{pq}E_{rs}T_{tu}^{(1,m')}|\Psi_{X}\rangle \tag{53}$$

where m + m' = 0. This is equivalent in cost to measuring a 4-particle reduced density matrix.

AUTHOR INFORMATION

Corresponding Author

Emiel Koridon – Instituut-Lorentz, Universiteit Leiden, Leiden 2300RA, The Netherlands; Theoretical Chemistry, Vrije Universiteit, Amsterdam 1081HV, The Netherlands; orcid.org/0000-0002-7712-7638; Email: koridon@lorentz.leidenuniv.nl

Authors

Souloke Sen – Instituut-Lorentz, Universiteit Leiden, Leiden 2300RA, The Netherlands; Theoretical Chemistry, Vrije Universiteit, Amsterdam 1081HV, The Netherlands

Lucas Visscher – Theoretical Chemistry, Vrije Universiteit, Amsterdam 1081HV, The Netherlands; orcid.org/0000-0002-7748-6243

Stefano Polla – Instituut-Lorentz, Universiteit Leiden, Leiden 2300RA, The Netherlands

Complete contact information is available at: https://pubs.acs.org/10.1021/acs.jctc.4c01221

Notes

The authors declare no competing financial interest.

ACKNOWLEDGMENTS

We thank Dr. Arno Förster, Sarathchandra Khandavilli, and Detlef Hohl for stimulating discussions. We thank Seenivasan Hariharan and Matthias Degroote for useful feedback. We acknowledge support from Shell Global Solutions BV.

REFERENCES

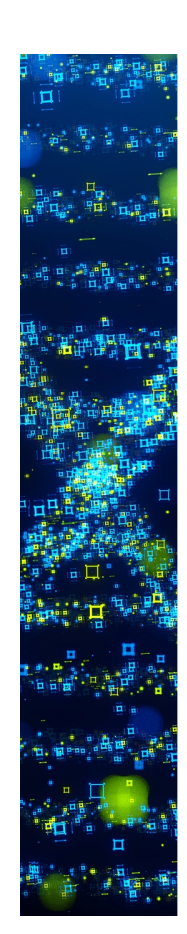
- (1) Park, J. W.; Al-Saadon, R.; MacLeod, M. K.; Shiozaki, T.; Vlaisavljevich, B. Multireference electron correlation methods: Journeys along potential energy surfaces. *Chem. Rev.* **2020**, *120*, 5878–5909.
- (2) Szalay, P. G.; Muller, T.; Gidofalvi, G.; Lischka, H.; Shepard, R. Multiconfiguration self-consistent field and multireference configuration interaction methods and applications. *Chem. Rev.* **2012**, *112*, 108–181.
- (3) Roos, B. O.; et al. The complete active space self-consistent field method and its applications in electronic structure calculations. *Adv. Chem. Phys.* **1987**, *69*, 399–445.
- (4) Olsen, J.; Roos, B. O.; Jo/Rgensen, P.; Jensen, H. J. A. Determinant based configuration interaction algorithms for complete and restricted configuration interaction spaces. *J. Chem. Phys.* **1988**, 89 (4), 2185–2192.
- (5) Malmqvist, P. Å.; Rendell, A.; Roos, B. O. The restricted active space self-consistent-field method, implemented with a split graph unitary group approach. *J. Phys. Chem.* **1990**, *94*, 5477–5482.
- (6) Fleig, T.; Olsen, J.; Visscher, L. The generalized active space concept for the relativistic treatment of electron correlation. II. Large-scale configuration interaction implementation based on relativistic 2-and 4-spinors and its application. *J. Chem. Phys.* **2003**, *119*, 2963–2971
- (7) Ma, D.; Manni, G. L.; Gagliardi, L. The generalized active space concept in multiconfigurational self-consistent field methods. *J. Chem. Phys.* **2011**, *135* (4), 044128.
- (8) Manni, G. L.; Aquilante, F.; Gagliardi, L. Strong correlation treated via effective hamiltonians and perturbation theory. *J. Chem. Phys.* **2011**, *134* (3), 034114.
- (9) Li Manni, G.; Ma, D.; Aquilante, F.; Olsen, J.; Gagliardi, L. SplitGAS method for strong correlation and the challenging case of Cr2. *J. Chem. Theory Comput.* **2013**, *9*, 3375–3384.
- (10) Smith, J. E.; Mussard, B.; Holmes, A. A.; Sharma, S. Cheap and near exact CASSCF with large active spaces. *J. Chem. Theory Comput.* **2017**, *13*, 5468–5478.
- (11) Levine, D. S.; Hait, D.; Tubman, N. M.; Lehtola, S.; Whaley, K. B.; Head-Gordon, M. CASSCF with extremely large active spaces using the adaptive sampling configuration interaction method. *J. Chem. Theory Comput.* **2020**, *16*, 2340–2354.

- (12) Baiardi, A.; Reiher, M. The Density Matrix Renormalization Group in Chemistry and Molecular Physics: Recent Developments and New Challenges. *J. Chem. Phys.* **2020**, *152* (4), 040903.
- (13) Austin, B. M.; Zubarev, D. Y.; Lester, W. A. J. Quantum Monte Carlo and Related Approaches. *Chem. Rev.* **2012**, *112*, 263–288.
- (14) Bauer, B.; Bravyi, S.; Motta, M.; Chan, G. K.-L. Quantum Algorithms for Quantum Chemistry and Quantum Materials Science. *Chem. Rev.* **2020**, *120*, *12685*–*12717*.
- (15) Gordon, M. S.; Fedorov, D. G.; Pruitt, S. R.; Slipchenko, L. V. Fragmentation methods: A route to accurate calculations on large systems. *Chem. Rev.* **2012**, *112*, 632–672.
- (16) Collins, M. A.; Bettens, R. P. Energy-based molecular fragmentation methods. *Chem. Rev.* **2015**, *115*, 5607–5642.
- (17) Raghavachari, K.; Saha, A. Accurate composite and fragment-based quantum chemical models for large molecules. *Chem. Rev.* **2015**, *115*, 5643–5677.
- (18) Fedorov, D. G.; Alexeev, Y.; Kitaura, K. Geometry optimization of the active site of a large system with the fragment molecular orbital method. *J. Phys. Chem. Lett.* **2011**, *2*, 282–288.
- (19) Knizia, G.; Chan, G. K.-L. Density matrix embedding: A simple alternative to dynamical mean-field theory. *Phys. Rev. Lett.* **2012**, *109*, 186404.
- (20) Knizia, G.; Chan, G. K.-L. Density matrix embedding: A strong-coupling quantum embedding theory. *J. Chem. Theory Comput.* **2013**, *9*, 1428–1432.
- (21) Bulik, I. W.; Scuseria, G. E.; Dukelsky, J. Density matrix embedding from broken symmetry lattice mean fields. *Phys. Rev. B* **2014**, *89*, 035140.
- (22) Yalouz, S.; Sekaran, S.; Fromager, E.; Saubanère, M. Quantum Embedding of Multi-Orbital Fragments Using the Block-Householder Transformation. *J. Chem. Phys.* **2022**, *157* (21), 214112.
- (23) Bulik, I. W.; Chen, W.; Scuseria, G. E. Electron correlation in solids via density embedding theory. *J. Chem. Phys.* **2014**, *141* (5), 054113.
- (24) Wouters, S.; Jiménez-Hoyos, C. A.; Sun, Q.; Chan, G. K.-L. A practical guide to density matrix embedding theory in quantum chemistry. *J. Chem. Theory Comput.* **2016**, *12*, 2706–2719.
- (25) Pham, H. Q.; Bernales, V.; Gagliardi, L. Can density matrix embedding theory with the complete activate space self-consistent field solver describe single and double bond breaking in molecular systems? *J. Chem. Theory Comput.* **2018**, *14*, 1960–1968.
- (26) Zheng, B.-X.; Chan, G. K.-L. Ground-state phase diagram of the square lattice Hubbard model from density matrix embedding theory. *Phys. Rev. B* **2016**, *93*, 035126.
- (27) Chen, Q.; Booth, G. H.; Sharma, S.; Knizia, G.; Chan, G. K.-L. Intermediate and spin-liquid phase of the half-filled honeycomb Hubbard model. *Phys. Rev. B* **2014**, *89*, 165134.
- (28) Zheng, B.-X.; Kretchmer, J. S.; Shi, H.; Zhang, S.; Chan, G. K.-L. Cluster size convergence of the density matrix embedding theory and its dynamical cluster formulation: A study with an auxiliary-field quantum Monte Carlo solver. *Phys. Rev. B* **2017**, *95*, 045103.
- (29) Jones, L. O.; Mosquera, M. A.; Schatz, G. C.; Ratner, M. A. Embedding methods for quantum chemistry: applications from materials to life sciences. *J. Am. Chem. Soc.* **2020**, *142*, 3281–3295.
- (30) Sen, S. Computational Studies Of Excited States Of Chlorophyll Dimers In Light-Harvesting Complexes. PhD-Thesis Research And Graduation Internal; Vrije Universiteit Amsterdam, 2023.
- (31) Parker, S. M.; Seideman, T.; Ratner, M. A.; Shiozaki, T. Communication: Active-space decomposition for molecular dimers. *J. Chem. Phys.* **2013**, *139* (2), 021108.
- (32) Jiménez-Hoyos, C. A.; Scuseria, G. E. Cluster-based mean-field and perturbative description of strongly correlated fermion systems: Application to the one-and two-dimensional Hubbard model. *Phys. Rev. B* **2015**, 92, 085101.
- (33) Hermes, M. R.; Gagliardi, L. Multiconfigurational self-consistent field theory with density matrix embedding: The localized active space self-consistent field method. *J. Chem. Theory Comput.* **2019**, *15*, 972–986.

- (34) Hermes, M. R.; Pandharkar, R.; Gagliardi, L. Variational Localized Active Space Self-Consistent Field Method. *J. Chem. Theory Comput.* **2020**, *16*, 4923–4937.
- (35) Rummel, L.; Schreiner, P. R. Advances and Prospects in Understanding London Dispersion Interactions in Molecular Chemistry. *Angew. Chem., Int. Ed.* **2024**, *63* (12), No. e202316364.
- (36) Schrödinger, E. Quantisierung als eigenwertproblem. *Ann. Phys.* **1926**, 385, 437–490.
- (37) Andersson, K.; Malmqvist, P. A.; Roos, B. O.; Sadlej, A. J.; Wolinski, K. Second-Order Perturbation Theory with a CASSCF Reference Function. *J. Phys. Chem.* **1990**, *94*, 5483–5488.
- (38) Angeli, C.; Cimiraglia, R.; Evangelisti, S.; Leininger, T.; Malrieu, J.-P. Introduction of n-electron valence states for multi-reference perturbation theory. *J. Chem. Phys.* **2001**, *114*, 10252–10264.
- (39) Angeli, C.; Cimiraglia, R.; Malrieu, J.-P. n-electron valence state perturbation theory: A spinless formulation and an efficient implementation of the strongly contracted and of the partially contracted variants. *J. Chem. Phys.* **2002**, *117*, 9138–9153.
- (40) Abraham, V.; Mayhall, N. J. Selected configuration interaction in a basis of cluster state tensor products. *J. Chem. Theory Comput.* **2020**, *16*, 6098–6113.
- (41) Hapka, M.; Przybytek, M.; Pernal, K. Symmetry-adapted perturbation theory based on multiconfigurational wave function description of monomers. *J. Chem. Theory Comput.* **2021**, *17*, 5538–5555.
- (42) Papastathopoulos-Katsaros, A.; Jiménez-Hoyos, C. A.; Henderson, T. M.; Scuseria, G. E. Coupled cluster and perturbation theories based on a cluster mean-field reference applied to strongly correlated spin systems. *J. Chem. Theory Comput.* **2022**, *18*, 4293–4303.
- (43) Xu, E.; Li, S. Block correlated second order perturbation theory with a generalized valence bond reference function. *J. Chem. Phys.* **2013**, *139* (17), 174111.
- (44) Wang, Q.; Duan, M.; Xu, E.; Zou, J.; Li, S. Describing strong correlation with block-correlated coupled cluster theory. *J. Phys. Chem. Lett.* **2020**, *11*, 7536–7543.
- (45) He, N.; Evangelista, F. A. A zeroth-order active-space frozen-orbital embedding scheme for multireference calculations. *J. Chem. Phys.* **2020**, *152* (9), 094107.
- (46) Coughtrie, D. J.; Giereth, R.; Kats, D.; Werner, H.-J.; Köhn, A. Embedded multireference coupled cluster theory. *J. Chem. Theory Comput.* **2018**, *14*, 693–709.
- (47) Otten, M.; Hermes, M. R.; Pandharkar, R.; Alexeev, Y.; Gray, S. K.; Gagliardi, L. Localized quantum chemistry on quantum computers. J. Chem. Theory Comput. 2022, 18, 7205–7217.
- (48) Senjean, B.; Sen, S.; Repisky, M.; Knizia, G.; Visscher, L. Generalization of Intrinsic Orbitals to Kramers-Paired Quaternion Spinors, Molecular Fragments, and Valence Virtual Spinors. *J. Chem. Theory Comput.* **2021**, *17*, 1337–1354.
- (49) Sen, S.; Senjean, B.; Visscher, L. Characterization of Excited States in Time-Dependent Density Functional Theory Using Localized Molecular Orbitals. J. Chem. Phys. 2023, 158 (5), 054115.
- (50) Pipek, J.; Mezey, P. G. A fast intrinsic localization procedure applicable for ab initio and semiempirical linear combination of atomic orbital wave functions. *J. Chem. Phys.* **1989**, *90*, 4916–4926.
- (51) Yarkony, D.; Silbey, R. The band gap in linear polyenes. *Chem. Phys.* **1977**, 20, 183–195.
- (52) Ghosh, D.; Hachmann, J.; Yanai, T.; Chan, G. K.-L. Orbital optimization in the density matrix renormalization group, with applications to polyenes and β-carotene. *J. Chem. Phys.* **2008**, *128* (14), 144117.
- (53) Marder, S. R.; Torruellas, W. E.; Blanchard-Desce, M.; Ricci, V.; Stegeman, G. I.; Gilmour, S.; Bredas, J.-L.; Li, J.; Bublitz, G. U.; Boxer, S. G. Large molecular third-order optical nonlinearities in polarized carotenoids. *Science* **1997**, *276*, 1233–1236.
- (54) Christensen, R. L.; Barney, E. A.; Broene, R. D.; Galinato, M. G. I.; Frank, H. A. Linear polyenes: models for the spectroscopy and

- photophysics of carotenoids. Arch. Biochem. Biophys. **2004**, 430, 30–36.
- (55) Barrett, A. G.; Ma, T.-K.; Mies, T. Recent developments in polyene cyclizations and their applications in natural product synthesis. *Synthesis* **2019**, *51*, *67*–82.
- (56) Senjean, B.; Sen, S.; Repisky, M.; Knizia, G.; Visscher, L. https://gitlab.com/quantum_rose, 2020.
- (57) Sun, Q.; Zhang, X.; Banerjee, S.; Bao, P.; Barbry, M.; Blunt, N. S.; Bogdanov, N. A.; Booth, G. H.; Chen, J.; Cui, Z.-H.; et al. Recent Developments in the PySCF Program Package. *J. Chem. Phys.* **2020**, 153 (2), 024109.
- (58) Sanfeliciano, S. M. G.; Schaus, J. M. Rapid assessment of conformational preferences in biaryl and aryl carbonyl fragments. *PLoS One* **2018**, *13* (3), No. e0192974. Publisher: Public Library of Science.
- (59) Mosher, O. A.; Flicker, W. M.; Kuppermann, A. Triplet states in 1, 3-butadiene. *Chem. Phys. Lett.* **1973**, *19*, 332–333.
- (60) Guo, Y.; Sivalingam, K.; Neese, F. Approximations of density matrices in N-electron valence state second-order perturbation theory (NEVPT2). I. Revisiting the NEVPT2 construction. *J. Chem. Phys.* **2021**, *154* (21), 214111.
- (61) Guo, Y.; Sivalingam, K.; Kollmar, C.; Neese, F. Approximations of density matrices in N-electron valence state second-order perturbation theory (NEVPT2). II. The full rank NEVPT2 (FRNEVPT2) formulation. *J. Chem. Phys.* **2021**, *154* (21), 214113.
- (62) Eichkorn, K.; Treutler, O.; Öhm, H.; Häser, M.; Ahlrichs, R. Auxiliary basis sets to approximate Coulomb potentials. *Chem. Phys. Lett.* **1995**, 240, 283–290.
- (63) Zgid, D.; Ghosh, D.; Neuscamman, E.; Chan, G. K.-L. A study of cumulant approximations to n-electron valence multireference perturbation theory. *J. Chem. Phys.* **2009**, *130* (19), 194107.
- (64) Kollmar, C.; Sivalingam, K.; Guo, Y.; Neese, F. An efficient implementation of the NEVPT2 and CASPT2 methods avoiding higher-order density matrices. *J. Chem. Phys.* **2021**, *155* (23), 234104.
- (65) Chatterjee, K.; Sokolov, A. Y. Extended Second-Order Multireference Algebraic Diagrammatic Construction Theory for Charged Excitations. *J. Chem. Theory Comput.* **2020**, *16*, 6343–6357.
- (66) Cioslowski, J. Connected moments expansion: A new tool for quantum many-body theory. *Phys. Rev. Lett.* **1987**, *58*, 83–85.
- (67) Mahajan, A.; Blunt, N. S.; Sabzevari, I.; Sharma, S. Multireference configuration interaction and perturbation theory without reduced density matrices. *J. Chem. Phys.* **2019**, *151* (21), 211102.
- (68) Blunt, N. S.; Mahajan, A.; Sharma, S. Efficient multireference perturbation theory without high-order reduced density matrices. *J. Chem. Phys.* **2020**, *153* (16), 164120.
- (69) Anderson, R. J.; Shiozaki, T.; Booth, G. H. Efficient and stochastic multireference perturbation theory for large active spaces within a full configuration interaction quantum Monte Carlo framework. *J. Chem. Phys.* **2020**, *152* (5), 054101.
- (70) Malone, F. D.; Parrish, R. M.; Welden, A. R.; Fox, T.; Degroote, M.; Kyoseva, E.; Moll, N.; Santagati, R.; Streif, M. Towards the Simulation of Large Scale Protein—Ligand Interactions on NISQ-era Quantum Computers. *Chem. Sci.* **2022**, *13*, 3094—3108.
- (71) Loipersberger, M.; Malone, F. D.; Welden, A. R.; Parrish, R. M.; Fox, T.; Degroote, M.; Kyoseva, E.; Moll, N.; Santagati, R.; Streif, M. Interaction Energies on Noisy Intermediate-Scale Quantum Computers. *arXiv*, **2022**.
- (72) Cortes, C. L.; Loipersberger, M.; Parrish, R. M.; Morley-Short, S.; Pol, W.; Sim, S.; Steudtner, M.; Tautermann, C. S.; Degroote, M.; Moll, N.; Santagati, R.; Streif, M. Fault-Tolerant Quantum Algorithm for Symmetry-Adapted Perturbation Theory. *PRX Quantum.* **2024**, 5 (1), 010336.
- (73) Mitra, A.; D'Cunha, R.; Wang, Q.; Hermes, M. R.; Alexeev, Y.; Gray, S. K.; Otten, M.; Gagliardi, L. The Localized Active Space Method with Unitary Selective Coupled Cluster. *J. Chem. Theory Comput.* **2024**, *20*, 7865–7875.
- (74) Peruzzo, A.; McClean, J. R.; Shadbolt, P.; Yung, M.-H.; Zhou, X.-Q.; Love, P. J.; Aspuru-Guzik, A.; O'Brien, J. L. A Variational

- Eigenvalue Solver on a Photonic Quantum Processor. *Nat. Commun.* **2014**, *5*, 4213.
- (75) McClean, J. R.; Romero, J.; Babbush, R.; Aspuru-Guzik, A. The Theory of Variational Hybrid Quantum-Classical Algorithms. *New J. Phys.* **2016**, *18*, 023023.
- (76) Bartlett, R. J.; Kucharski, S. A.; Noga, J. Alternative Coupled-Cluster Ansätze II. The Unitary Coupled-Cluster Method. *Chem. Phys. Lett.* **1989**, *155*, 133–140.
- (77) Grimsley, H. R.; Economou, S. E.; Barnes, E.; Mayhall, N. J. An Adaptive Variational Algorithm for Exact Molecular Simulations on a Quantum Computer. *Nat. Commun.* **2019**, *10* (1), 3007.
- (78) Anselmetti, G.-L. R.; Wierichs, D.; Gogolin, C.; Parrish, R. M. Local, Expressive, Quantum-Number-Preserving VQE Ansätze for Fermionic Systems. *New J. Phys.* **2021**, *23*, 113010.
- (79) Cerezo, M.; Arrasmith, A.; Babbush, R.; Benjamin, S. C.; Endo, S.; Fujii, K.; McClean, J. R.; Mitarai, K.; Yuan, X.; Cincio, L.; Coles, P. J. Variational Quantum Algorithms. *Nat. Rev. Phys.* **2021**, *3*, 625–644.
- (80) Tammaro, A.; Galli, D. E.; Rice, J. E.; Motta, M. N-Electron Valence Perturbation Theory with Reference Wave Functions from Quantum Computing: Application to the Relative Stability of Hydroxide Anion and Hydroxyl Radical. *J. Phys. Chem. A* 2023, 127, 817–827.
- (81) Krompiec, M.; Ramo, D. M. Strongly Contracted N-Electron Valence State Perturbation Theory Using Reduced Density Matrices from a Quantum Computer. *arxiv*, **2022**.
- (82) Bonet-Monroig, X.; Babbush, R.; O'Brien, T. E. Nearly Optimal Measurement Scheduling for Partial Tomography of Quantum States. *Phys. Rev. X* **2020**, *10*, 031064.
- (83) Huggins, W. J.; McClean, J. R.; Rubin, N. C.; Jiang, Z.; Wiebe, N.; Whaley, K. B.; Babbush, R. Efficient and Noise Resilient Measurements for Quantum Chemistry on Near-Term Quantum Computers. *Npj Quantum Inf.* **2021**, *7* (1), 23.
- (84) Huang, H.-Y.; Kueng, R.; Preskill, J. Predicting Many Properties of a Quantum System from Very Few Measurements. *Nat. Phys.* **2020**, *16*, 1050–1057.
- (85) Wan, K.; Huggins, W. J.; Lee, J.; Babbush, R. Matchgate Shadows for Fermionic Quantum Simulation. *Commun. Math. Phys.* **2023**, 404, 629–700.
- (86) Helgaker, T.; Jørgensen, P.; Olsen, J. Molecular Electronic-Structure Theory, 1ed Ed.; Wiley, 2000.
- (87) Szabo, A.; Ostlund, N. S. Modern Quantum Chemistry: introduction to Advanced Electronic Structure Theory, 1st ed. Ed.; Dover Publications, Inc.: Mineola, 1996.
- (88) Phipps, M. J.; Fox, T.; Tautermann, C. S.; Skylaris, C.-K. Energy decomposition analysis approaches and their evaluation on prototypical protein—drug interaction patterns. *Chem. Soc. Rev.* **2015**, 44, 3177–3211.
- (89) Albelda, M. T.; Frías, J. C.; García-Espana, E.; Schneider, H.-J. Supramolecular complexation for environmental control. *Chem. Soc. Rev.* **2012**, *41*, 3859–3877.
- (90) Sculfort, S.; Braunstein, P. Intramolecular d10–d10 interactions in heterometallic clusters of the transition metals. *Chem. Soc. Rev.* **2011**, *40*, 2741–2760.
- (91) Pyykkö, P.; Li, J.; Runeberg, N. Predicted ligand dependence of the Au (I)...u (I) attraction in (XAuPH3) 2. *Chem. Phys. Lett.* **1994**, 218, 133–138.
- (92) Otero-de-la Roza, A.; Mallory, J. D.; Johnson, E. R. Metallophilic interactions from dispersion-corrected density-functional theory. *J. Chem. Phys.* **2014**, *140* (18), 18A504.



CAS BIOFINDER DISCOVERY PLATFORM™

STOP DIGGING THROUGH DATA —START MAKING DISCOVERIES

CAS BioFinder helps you find the right biological insights in seconds

Start your search

